A STUDY OF HIGH ENERGY NEUTRON DETECTORS

E. R. Christie

DET	DETECTOR
ENE	ENERGY
NEU	NEUTRON

A STUDY OF HIGH ENERGY NEUTRON DETECTORS

by

E. R. CHRISTIE

B. S., Ohio University

1948

SUBMITTED IN PARTIAL FULFILLMENT
OF THE REQUIREMENTS FOR THE
DEGREE OF MASTER OF
SCIENCE

at the

MASSACHUSETTS INSTITUTE OF

A STUDY OF HIGH ENERGY NEUTRON DETECTORS

by

E. R. CHRISTIE
B. S., Ohio University
1948

SUBMITTED IN PARTIAL FULFILLMENT
OF THE REQUIREMENTS FOR THE
DEGREE OF MASTER OF
SCIENCE
at the
MASSACHUSETTS INSTITUTE OF
TECHNOLOGY
June, 1955

STUDY OF HIGH ENERGY NEUTRON DETECTORS

by

T. R. CHRISTIE

SUBMITTED TO THE DEPARTMENT OF PHYSICS
ON 23 MAY 1955 IN PARTIAL FULFILLMENT
OF THE REQUIREMENTS FOR THE DEGREE OF
MASTER OF SCIENCE

Two neutron counters employing liquid scintillators have been used to detect neutrons of 70 to 170 Mev energy. One counter was a cylinder twelve inches long by four inches in diameter. It was used to obtain angular distributions of energetic neutrons. The other counter was in the shape of a dish five inches thick with a diameter of twenty two to thirty two inches. It was used in experiments where large solid angle coverage was desired.

Both counters were studied experimentally in detail. The photodisintegration of the deuteron was used as a (monoergic) source of neutrons to investigate the behavior of the counters. The angular resolution and efficiency of the counters were determined as a function of neutron energy, geometry, target thickness and position, neutron bias energy, lead shielding, and neutron counter size.

A method of theoretical analysis of the above factors is developed. The experimental results are compared with those from theoretical calculations. From the agreement obtained, the behavior of the small counter seems to be very well understood. The values of absolute efficiency calculated for the large counter are not in complete agreement with those obtained experimentally. Reasonable assumptions concerning the cause of these discrepancies are advanced which lead to a qualitative agreement.

A survey of alternate methods of high energy neutron detection is included.

Thesis Supervisor.....Bernard T. Feld
Associate Professor of Physics

The author wishes to acknowledge his indebtedness to Dr. Wattenberg and Dr. Feld for their guidance, interest, and inspiration; to A. C. Odian who assembled the bulk of the apparatus used in this study; and to the others in the group for their assistance and a very pleasant association: W. Rankin, P. Stein, R. Weinstein, and H. Wilson.

The author wishes to acknowledge his indebtedness to Dr. Wattenberg and Dr. Feld for their guidance, interest, and inspiration; to A. C. Odlum who assembled the bulk of the apparatus used in this study; and to the others in the group for their assistance and a very pleasant association: W. Rankin, P. Stein, R. Weinstein, and R. Wilson.

TABLE OF CONTENTS

I. INTRODUCTION

Investigations of High Energy Photoproton production by 325 Mev Bremsstrahlung Radiation by Feld et al[1] and Neutrons in Coincidence with High Energy Photoprotons by H. Meyers et al[2] have been conducted at the M.I.T. Synchrotron Laboratory. Similar experiments have been undertaken at other laboratories.[3] These investigations indicated that there was substantial evidence that the process involved in photoproton production was the photodisintegration of neutron-proton pairs, i.e. deuteron-like subunits in the nucleus as proposed by Levinger.[4] Further investigation was deemed warranted and has indicated this to be the case.[5]

Inasmuch as the high energy neutron detectors under discussion in this paper were employed in the latter investigations, a brief outline of the experiment would seem to be in order.

Targets of various nuclei were placed in the bremsstrahlung beam of the M.I.T. synchrotron. As the process being investigated is essentially a two body problem one observes this by detecting a neutron and proton in coincidence possessing the proper kinematic relationships. The proton telescope consisting of three plastic (Pilot Co.) scintillators and appropriate energy absorbers was placed at a desired angle. The electronics was biased to accept protons of a narrow energy spread ($\pm$12.5 Mev) about some selected proton energy. (For details concerning the proton telescope and techniques see references 1 and 5.) A neutron detector was placed at an angle appropriate to the energy and angle of the proton telescope. The signals from the proton telescope and the neutron detector were then fed through a fast coincidence circuit.

neutron detector were then fed through a fast coincidence circuit. the proton telescope. The signals from the proton telescope and the detector was placed at an angle appropriate to the energy and angle of the proton telescope and techniques see reference 1 and 5.) A neutron ($\pm$12.5 Mev) about some selected proton energy. (For details concerning The electronics was biased to accept protons of a narrow energy spread ator and appropriate energy absorbers was placed at a desired angle. The proton telescope consisting of three plastic (Pilot Co.) scintilproton in coincidence possessing the proper kinematic relationships. ially a two body problem one observes this by detecting a neutron and of the M.I.T. synchrotron. As the process being investigated is essentarget of various nuclei were placed in the bremsstrahlung beam

Inasmuch as the high energy neutron detectors under discussion in this paper were employed in the latter investigations, a brief outline of the experiment would seem to be in order.

was deemed warranted and has indicated this to be the case.

subunits in the nucleus as proposed by Levinger.[4] Further investigation was the photodisintegration of neutron-proton pairs, i.e. deuteron-like substantial evidence that the process involved in photoproton production at other laboratories.[3] These investigations indicated that there was M.I.T. Synchrotron laboratory. Similar experiments have been undertaken High energy Photoprotons by H. Meyers et al have been conducted at the

[2]

[1]

bremsstrahlung excitation by Gold et al and Neutrons in Coincidence with

[1] ... High Energy Photo Prot n Production by 325 ev

For a given proton angle, proton energy, neutron angle and γ ray energy, the problem of the photodisintegration of a deuteron is kinematically overdetermined. One observes neutron-proton coincidences over a small range of angles of the neutron counter. The spread in angle is a measure of the initial momenta of the nucleons involved. A series of experiments was undertaken to study the process further and to employ the process as a tool. Specifically it was desired to compare the momentum of nucleons in various nuclei.

These are experiments in which one gains additional information from absolute values; therefore a thorough understanding of all the factors effecting the operation and effeciency of the neutron detecting equipment was essential. This thesis is an experimental and theoretical study of the neutron counters employed.

A small neutron counter, "little neut", was used to obtain angular distributions and a large counter, referred to as "FS" or the "Flying Saucer", was used to obtain the integral values for total n+p events. The large counter is studied in detail in section III, theoretical calculations are compared with experimental results. The small counter is studied in section IV. Section II contains a general review of the types of instruments available for the detection of fast neutrons. Comments on the adaptability of these methods to the present n+p experiment are made and summarized in paragraph II,f.

for a given proton angle, proton energy, neutron angle and Q re-
energy, the problem of the photodisintegration of a deuteron is
kinematically overdetermined. One observes neutron-proton coin-
cidences over a small range of angles of the neutron counter. The
spread in angle is a measure of the initial momenta of the nucleons
involved. A series of experiments was undertaken to study the process
further and to employ the process as a tool. Specifically it was
desired to compare the momentum of nucleons in various nuclei.

These are experiments in which one gains additional information
from absolute values; therefore a thorough understanding of all the
factors effecting the operation and efficiency of the neutron detect-
ing equipment was essential. This thesis is an experimental and
theoretical study of the neutron counters employed.

A small neutron counter, "little nut", was used to obtain
angular distributions and a large counter, referred to as "BS" or
the "Flying Saucer", was used to obtain the integral values for total
n+p events. The large counter is studied in detail in section III,
theoretical calculations are compared with experimental results. The
small counter is studied in section IV. Section II contains a general
review of the types of instruments available for the detection of fast
neutrons. Comments on the adaptability of these methods to the present
n+p experiment are made and summarized in paragraph II,1.

II. DESCRIPTION OF TYPES OF NEUTRON DETECTORS

A. General

Since fast neutrons themselves produce only negligible ionization directly, their detection is dependent on their interaction with bodies whose effects can be detected. Usually this interaction consists of transferring all or part of the neutron energy to charged particles, chiefly the lighter nuclei, which may then be detected by their ionization. Since the cross section (total) for neutron interactions is in general small and a decreasing function of neutron energy[6,7] ($10 < E_{neut} < 200$ Mev), efficient detection of high energy neutrons is dependent on the incident neutron being confronted with a large number of nuclei with which to interact and whose interactions can be detected in the laboratory.

B. Ionization Chambers and Proportional Counters

These instruments have been employed with success as detectors of γ rays and are readily adaptable to the detection of neutrons since many of the problems involved in both types of detection are similar. These instruments measure the amount of ionization produced in a gaseous volume by the passage of charged particles. To detect fast neutrons they are usually filled with a hydrogenous gas under pressure.[8,9] The ions formed by the recoil protons are collected and measured. Since the mean path for neutrons of ~100 Mev in a medium of such low density is very large in comparison with the limits of physical size of any practical detector, these instruments are inherently of low efficiency for fast neutrons. Efficiencies of

A. General

Since fast neutrons themselves produce only negligible ionization directly, their detection is dependent on their interaction with bodies whose effects can be detected. Usually this interaction consists of transferring all or part of the neutron energy to charged particles, chiefly the lighter nuclei, which may then be detected by their ionization. Since the cross section (total) for neutron interactions is in general small and a decreasing function of neutron energy, efficient detection of high energy neutrons is dependent on the incident neutron being confronted with a large number of nuclei with which to interact and whose interactions can be detected in the laboratory.

B. Ionization Chambers and Proportional Counters

These instruments have been employed with success as detectors of γ rays and are readily adaptable to the detection of neutrons since many of the problems involved in both types of detection are similar. These instruments measure the amount of ionization produced in a gaseous volume by the passage of charged particles. To detect fast neutrons they are usually filled with a hydrogenous gas under pressure. The ions formed by the recoil protons are collected and measured. Since the mean path for neutrons of ~100 Mev in a medium of such low density is very large in comparison with the limits of physical size of any practical detector, these instruments are inherently of low efficiency for fast neutrons. Efficiencies of

the order of 10% have been possible with low energy neutrons[8] (2.3 Mev), electron collection times are one microsecond. Efficiency of neutrons ~100 Mev is reduced to the order of 10^{-3}.

Efficiencies of these instruments have been increased, at the expense of greater ion collection times (~seconds), by the use of insulating liquids such as hexane and decane under field strengths of up to 1000 volts/cm.[10] Thin hydrogenous targets can be placed in front of or inside of these counters to increasd the probability of a recoil proton.[11]

Because of their low efficiencies for fast neutrons and relatively slow response time for fast coincidence work such detectors were not employed in these experiments.

C. Cloud Chambers and Photographic Emulsions

These instruments are mentioned only briefly for completeness as they are not efficiently adaptable to coincidence work. Cloud chambers utilizing a hydrogen atmosphere have been employed[12] to detect and measure the energy of neutrons of <1 Mev. If the direction of the incident neutron is known, its energy can be directly obtained from the length and direction of the recoil proton. In an analagous fashion photographic plates loaded with a hydrogenous material have been used to measure proton recoils employing standard plate techniques. Photographic plates loaded with various nuclei that possess threshold energies for neutron reactions can be used to detect and give minimum energies of neutrons. Keepin and Roberts have utilized the reaction $Li^6(n,\alpha)H^3$. The reaction $B^{10}(n,2\alpha)H^3$ has been suggested for

$Li^6(n,\alpha)H^3$. The reaction $B^{10}(n,2\alpha)H^3$ has been suggested for

energies of neutrons. Keepin and Roberts have utilized the reaction

energies for neutron reactions can be used to detect and give minimum

Photographic plates loaded with various nuclei that possess threshold

been used to measure proton recoils employing standard plate techniques.

fission photographic plates loaded with a hydrogenous material have

from the length and direction of the recoil proton. In an analogous

of the incident neutron is known, its energy can be directly obtained

tect and measure the energy of neutrons of <1 Mev. If the direction

chambers utilizing a hydrogen atmosphere have been employed to de-

as they are not efficiently adaptable to coincidence work. Cloud

These instruments are mentioned only briefly for completeness

6. Cloud Chambers and Photographic Emulsions

employed in these experiments.

slow response time for fast coincidence work such detectors were not

Because of their low efficiencies for fast neutrons and relatively

proton.

of or inside of these counters to increased the probability of a recoil

up to 1000 volts/cm. Thin hydrogenous targets can be placed in front

insulating liquids such as hexane and decane under field strengths of

expense of greater ion collection times (~seconds), by the use of

Efficiencies of these instruments have been increased, at the

~100 Mev is reduced to the order of 10^{-3}.

electron collection times are one microsecond. Efficiency of neutrons

e order of 10% have been possible with low energy neutrons (2.3 Mev),

neutrons of greater than 10 Mev.

D. Fission Chambers

Uranium fission chambers have been used with success to detect neutrons in the range $\leq$15 Mev. Some workers [14,15] have employed bismuth fission chambers for neutron energies $<$ 50 Mev. The efficiency of such detectors is normally about 10^{-4} or less.

E. Scintillation Detectors

1. General

Scintillation counters have supplanted most other types of counters for detecting all kinds of radiations. Some transparent condensed material that is capable of producing observable light pulses following internal ionization is used. These light pulses are detected and amplified by means of photomultiplier tubes. Neutrons are detected by observing recoiling charged particles.

2. Types of Scintillation Detectors

a. Organic Crystals

Organic crystals such as anthracene and stilbene have been used to detect neutrons by means of light pulses produced by recoiling protons. The crystals are very transparent and produce relatively large light pulses. In practice, the high cost and the manufacturing difficulties incident to making high grade crystals of large enough size for high energy neutron work limit their use in the laboratory for this purpose.

The newer plastic scintillators could conceivably be used in this manner. They are expensive in large sizes.

c. Ionization Chambers

Uranium ionization chambers have been used with success to detect neutrons in the range <15 Mev. Some workers [illegible] have employed bismuth ionization chambers for neutron energies < 50 Mev. The efficiency of such detectors is normally about 10^{-4} or less.

B. Scintillation Detectors

1. General

Scintillation counters have supplanted most other types of counters for detecting all kinds of radiations. Some transparent condensed material that is capable of producing observable light pulses following internal ionization is used. These light pulses are detected and amplified by means of photomultiplier tubes. Neutrons are detected by observing recoiling charged particles.

2. Types of Scintillation Detectors

a. Organic Crystals

Organic crystals such as anthracene and stilbene have been used to detect neutrons by means of light pulses produced by recoiling protons. The crystals are very transparent and produce relatively large light pulses. In practice, the high cost and the manufacturing difficulties incident to making high grade crystals of large enough size for high energy neutron work limit their use in the laboratory for this purpose.

The newer plastic scintillators could conceivably be used in this manner. They are expensive in large sizes.

b. Liquid Scintillators

The relative merits of various liquid organic compounds when used as scintillating media have been measured.[16] Neutron detection is accomplished as before by observing the light pulses produced by recoiling protons. The light output per unit energy loss in the scintillator is somewhat less for the liquid scintillators than for the crystals; however, they are readily available from commercial sources at relatively low cost, very transparent, and can be contained in a detector of arbitrary size and shape. The liquid scintillators appear to be the most advantageous for high energy neutron detection as their transparency allows good light collection even when the counter size is commensurate with the mean path for fast neutrons. Their fast response[17] facilitates coincidence work and allows the use of high absolute counting rates.

3. Scintillation Counters and Determination of Neutron Energy

a. Analysis of Recoil Proton Spectrum

If the relationship between the amount of light produced in the scintillator were linear with the energy loss of the recoiling proton, the proton spectrum yielded by monoergic neutrons would be flat from zero out to the energy of the incident neutrons. This assumes isotropic n-p scattering. The neutron spectrum would simply be the derivative of this spectrum, i.e., a spike at E_n. In general, the derivative of the proton spectrum would yield the neutron spectrum for purely recoil events.

b. Liquid Scintillators

The relative merits of various liquid organic compounds when used as scintillating media have been measured. [16] Neutron detection is accomplished as before by observing the light pulses produced by recoiling protons. The light output per unit energy loss in the scintillator is somewhat less for the liquid scintillators than for the crystals; however, they are readily available from commercial sources at relatively low cost, very transparent, and can be contained in a detector of arbitrary size and shape. The liquid scintillators appear to be the most advantageous for high energy neutron detection as their transparency allows good light collection even when the counter size is commensurate with the mean path for fast neutrons. Their fast response facilitates coincidence work and allows the use of high [17] absolute counting rates.

3. Scintillation Counters and Determination of Neutron Energy

a. Analysis of Recoil Proton Spectrum

If the relationship between the amount of light produced in the scintillator were linear with the energy loss of the recoiling proton, the proton spectrum yielded by monoenergic neutrons would be flat from zero out to the energy of the incident neutrons. This assumes isotropic n-p scattering. The neutron spectrum would simply be the derivative of this spectrum, i.e., a spike at E_n. In general, the derivative of the proton spectrum would yield the neutron spectrum for purely recoil events.

Unfortunately the relationship between light output and proton energy loss is not linear at low proton energies and must be taken into account. The theoretical curves of Birks,[18] which are in general agreement with the data of Taylor et al,[19] give this relationship. These curves, which are for anthracene, are assumed here to apply to the other organic scintillators in the non-linear region below 15 Mev.

Another difficulty in the analysis of the proton pulse spectrum is that at high neutron energies ~90 Mev, energetic protons and other charged particles are ejected from the carbon nuclei present in the liquid (i.e. one observes stars and spallation). At these energies, the cross section for such contributions from the carbon is commensurate with and may be greater than the cross section for n-p scattering.[20,21]

A further complication in the analysis of the recoil proton spectrum is that the n-p scattering can no longer be considered to be simply s wave scattering (isotropic) at neutron energies in excess of 14 Mev. Data concerning the anisotropy of n-p scattering at neutron energies of 40,90 and 260 Mev is given by Kelly et al.[22]

The analysis of the recoil proton spectrum to obtain the incident neutron spectrum is difficult to do analytically. The problem is amenable to numerical methods, such as the Monte Carlo[23,24] technique, if one merely wishes to verify an assumed neutron spectrum.

primarily the relation ship between light output and proton

energy does in not linear at low proton energies and must be taken

into account. The theoretical curves of Birks[18], which are in general

agreement with the data of Taylor et al.[19] give this relationship. These

curves, which are for anthracene, are assumed here to apply to the other

organic scintillators in the non-linear region below 15 Mev.

Another difficulty in the analysis of the proton pulse spectrum

is that at high neutron energies ~20 Mev, energetic protons and other

charged particles are ejected from the carbon nuclei present in the

liquid (i.e. one observes stars and spallation). At these energies,

the cross section for such contributions from the carbon is comparable with and may be greater than the cross section for n-p scattering.[20,21]

A further complication in the analysis of the recoil proton

spectrum is that the n-p scattering can no longer be considered to

be simply a wave scattering (isotropic) at neutron energies in excess

of 11 Mev. Data concerning the anisotropy of n-p scattering at neu-

tron energies of 10,20 and 260 Mev is given by Kelly et al.[22]

The analysis of the recoil proton spectrum to obtain the in-

cident neutron spectrum is difficult to do analytically. The problem

is amenable to numerical methods, such as the Monte Carlo technique,[23,24]

if one merely wishes to verify an assumed neutron spectrum.

b. Utilization of N-P Scattering

(1) Neutron-Proton Coincidence Telescope

Several methods for measuring neutron energies are based on the kinematics of neutron-proton collisions. The neutron-proton telescope is one such method in which the neutrons to be detected are incident on an organic crystal which serves as an n-p scatterer and as a proton detector. A neutron detector is placed at a certain angle, coincidences between the neutron and proton counters define the angle of scattering and the pulse height of proton recoil yields the neutron energy directly. To keep the energy spread small, the angle of scattering must be well defined, thus this instrument is of low efficiency due to solid angle effects and the small n-p scattering cross section at high neutron energies. The latter factor is doubly weighted in view of the stringent conditions imposed on the incident neutron for detection. Namely that two separate neutron events occur, n-p scattering into a finite solid angle by the crystal and finally detection of the scattered neutron in the neutron counter. Its use has been successfully reported for neutrons up to 14 Mev.[25]

(2) "Thin"Proton Radiator and Proton Telescope

A second method of neutron energy determination employs a thin hydrogeneous radiator. Incident neutrons scatter protons forward into a proton telescope,[26] such as the one used in this experiment. The proton energy can be accurately measured. However, consideration of the conditions imposed on the thickness of the radiator and the solid angles show that it would be of low efficiency.

(2) "Thin"Proton Radiator and Proton Telescope

A second method of neutron energy determination employs a thin hydrogeneous radiator. Incident neutrons scatter protons forward into a proton telescope, such as the one used in this experiment. The proton energy can be accurately measured. However, consideration of the conditions imposed on the thickness of the radiator and the solid angles show that it would be of low efficiency.

has been successfully reported for neutrons up to 14 Mev.

detection of the scattered neutron in the neutron counter. Its use n-p scattering into a finite solid angle by the crystal and finally neutron for detection. Namely that two separate neutron events occur, weighted in view of the stringent conditions imposed on the incident cross section at high neutron energies. The latter factor is doubly low efficiency due to solid angle effects and the small n-p scattering angle of scattering must be well defined, thus this instrument is of the neutron energy directly. To keep the energy spread small, the angle of scattering and the pulse height of proton recoil yields and as a proton detector. A neutron detector is placed at a certain are incident on an organic crystal which serve as an n-p scatterer telescope is one such method in which the neutrons to be detected the kinematics of neutron-proton collisions. The neutron-proton several methods for measuring neutron energies are based on

(1) Auto-Proton Coincidence Telescope

An energy determination requires that only a small portion of the energy of the recoil protons originating in the radiator be lost in the radiator. Since the cross section for n-p scattering at high neutron energies is small, a thin radiator leads to a low probability that a recoil proton would be produced.

In order to have fairly monoergic recoils the proton must be scattered into a small solid angle. The small solid angle is another large factor in lowering the efficiency of such an instrument.

c. Neutron Detectors Based on the Total Absorbtion Principle

These instruments measure the total ionization produced as a high energy neutron is degraded in energy by successive scatterings in a large volume liquid scintillation detector. The pulses from individual scatterings are summed and are taken as an indication of the incident neutron energy. To insure that the neutron has given up all its energy to the scintillating liquid, the liquid is loaded with some material that has a very high cross section for thermal absorbtion of neutrons and which gives off an energetic γ ray (or other ionizing event) during the capture process. Only those initial recoil pulses are counted which are identified by a capture γ pulse occuring within a specified time after the initial pulse.

Cleland[27] has completed an evaluation study of such a detector employing Boron-10 capture for identification. Energies up to 14 Mev are considered and Monte Carlo sampling has been used to predict the efficiency and the energy resolution. A large volume detector employing cadmium for a capture γ pulse has been described by Reines et al.[28]

cadmium for a capture γ pulse has been described by Reines et al.[28]

efficiency and the energy resolution. A large volume detector employing are considered and Monte Carlo sampling has been used to predict the employing Boron-10 capture for identification. Energies up to 10 Mev

Cleland[27] has completed an evaluation study of such a detector

time after the initial pulse.

which are identified by a capture γ pulse occuring within a specified

the capture process. Only those initial recoil pulses are counted

and which gives off an energetic γ ray (or other ionizing event) during

that has a very high cross section for thermal absorption of neutrons

to the scintillating liquid, the liquid is loaded with some material

neutron energy. To insure that the neutron has given up all its energy

scatterings are summed and are taken as an indication of the incident

large volume liquid scintillation detector. The pulses from individual

energy neutron is degraded in energy by successive scatterings in a

These instruments measure the total ionization produced as a high

c. Neutron Detectors Based on the Total Absorption Principle

large factor in lowering the efficiency of such an instrument.

scattered into a small solid angle. The small solid angle is another

In order to have fairly monoergic recoils the proton must be

that a recoil proton would be produced.

neutron energies is small, a thin radiator leads to a low probability

in the radiator. Since the cross section for n-p scattering at high

the energy of the recoil protons originating in the radiator be lost

In general, a thin radiator is required so that only a small portion of

This type of instrument shows the most promise of being an efficient detector of high energy neutrons with good energy resolution.

C. Summary

The choice of a liquid scintillator for use in the neutron detectors in the n+p experiment was dictated by the following considerations:

1. Since the number of events to be recorded was small, the efficiency of the neutron counter must be high in order that the running time be minimized.

2. The resolving time for the detector system must be short in order to reduce accidental coincidences and to avoid pile up. This was especially important for the large counter since it was expected to have a high absolute counting rate of neutrons due to its size.

III. STUDY OF LARGE "FS" NEUTRON DETECTOR

A. Description of "FS"

Both counters employed as a scintillating liquid a mixture of 9 grams p-terphenyl per litre of phenylcyclohexane. To shift the wave length of the light pulses to the higher spectral response region of the photomultiplier tubes (RCA 5819), .03 grams per litre of Pilot Chemical Co. "Popop" was added. The physical properties of the solution were taken as:

Chemical formula	$C_6H_5C_6H_{11}$
Molecular weight	160.25
Density (20°C)	.944 grams/ml

The choice of a liquid scintillator for use in the neutron detector in the mtp experiment was dictated by the following considerations:

1. Since the number of events to be recorded was small, the efficiency of the neutron counter must be high in order that the running time be minimized.

2. The resolving time for the detector system must be short in order to reduce accidental coincidences and to avoid pile up. This was especially important for the large counter since it was expected to have a high absolute counting rate of neutrons due to its size.

III. STUDY OF LARGE "S" NEUTRON DETECTOR

A. Description of "S"

Both counters employed as a scintillating liquid a mixture of 5 grams p-terphenyl per litre of phenylcyclohexane. To shift the wave length of the light pulses to the higher spectral response region of the photomultiplier tubes (RCA 58AV), .03 grams per litre of Pilot Chemical Co. "Popop" was added. The physical properties of the solution were taken as:

Chemical formula	$C_6H_5C_6H_{11}$
Molecular weight	160.25
Density (20°C)	.946 grams/ml

The scintillating liquid is viewed from the back of the counter by nine RCA 5819 photomultiplier tubes. The tubes were mounted in 4" holes in optical contact with clear plastic windows. The FS counter was constructed of thin gauge sheet steel (~1/8") in the form of a truncated cone with an altitude of 5", back diameter 32", front diameter 22" (see figure 1). It was painted on the inside with titanium dioxide in water glass solution to provide a diffuse reflecting surface to aid in light collection and uniformity of response.

The high voltage of each tube was adjusted so that the gains of the photomultipliers were equal. The output signals from all nine tubes were added and fed to a cathode follower. The output of the cathode follower was fed to the circuit shown in figure 2. The FS was shielded from γ rays and other background by a 3" lead house. Accidental counts were determined by "teeing" the neutron detector signal and passing it through a 57 meter delay line. (See figure 2). The delay, .3 μ seconds, was long compared to the resolving time of the circuit. The delayed signal was then fed through a separate coincidence channel with the "teed" signal from the proton counter. The delay channel neutron signal was operated at a lower bias than the true coincidence neutron channel. The number of accidental coincidences subtracted was given by the product of the number of accidental coincidences registered times the ratio of the true coincidence neutron singles counting rate to the singles rate of those in the delayed channel.

The scintillation liquid is viewed from the back of the counter by five RCA 5521 photomultiplier tubes. The tubes were mounted in holes in optical contact with clear plastic windows. The 5" counter was constructed of thin gauge sheet steel (~1/8") in the form of a truncated cone with an altitude of 5", back diameter 32", front diameter 22" (see figure 1). It was painted on the inside with titanium dioxide in water glass solution to provide a diffuse reflecting surface to aid in light collection and uniformity of response.

The high voltage of each tube was adjusted so that the gains of the photomultipliers were equal. The output signals from all nine tubes were added and fed to a cathode follower. The output of the cathode follower was fed to the circuit shown in figure 2. The PS was shielded from γ rays and other background by a 3" lead house. Accidental counts were determined by "tseting" the neutron detector signal and passing it through a 57 meter delay line. (See figure 2). The delay, .3 μ seconds, was long compared to the resolving time of the circuit. The delayed signal was then fed through a separate coincidence channel with the "lead" signal from the proton counter. The delay channel neutron signal was operated at a lower bias than the true coincidence neutron channel. The number of accidental coincidences subtracted was given by the product of the number of accidental coincidences registered times the ratio of the true coincidence neutron singles counting rate to the singles rate of those in the delayed channel.

Figure 1: The Flying Saucer Neutron Counter

Figure 1.1 The Flying Saucer Neutron Counter

Figure 1

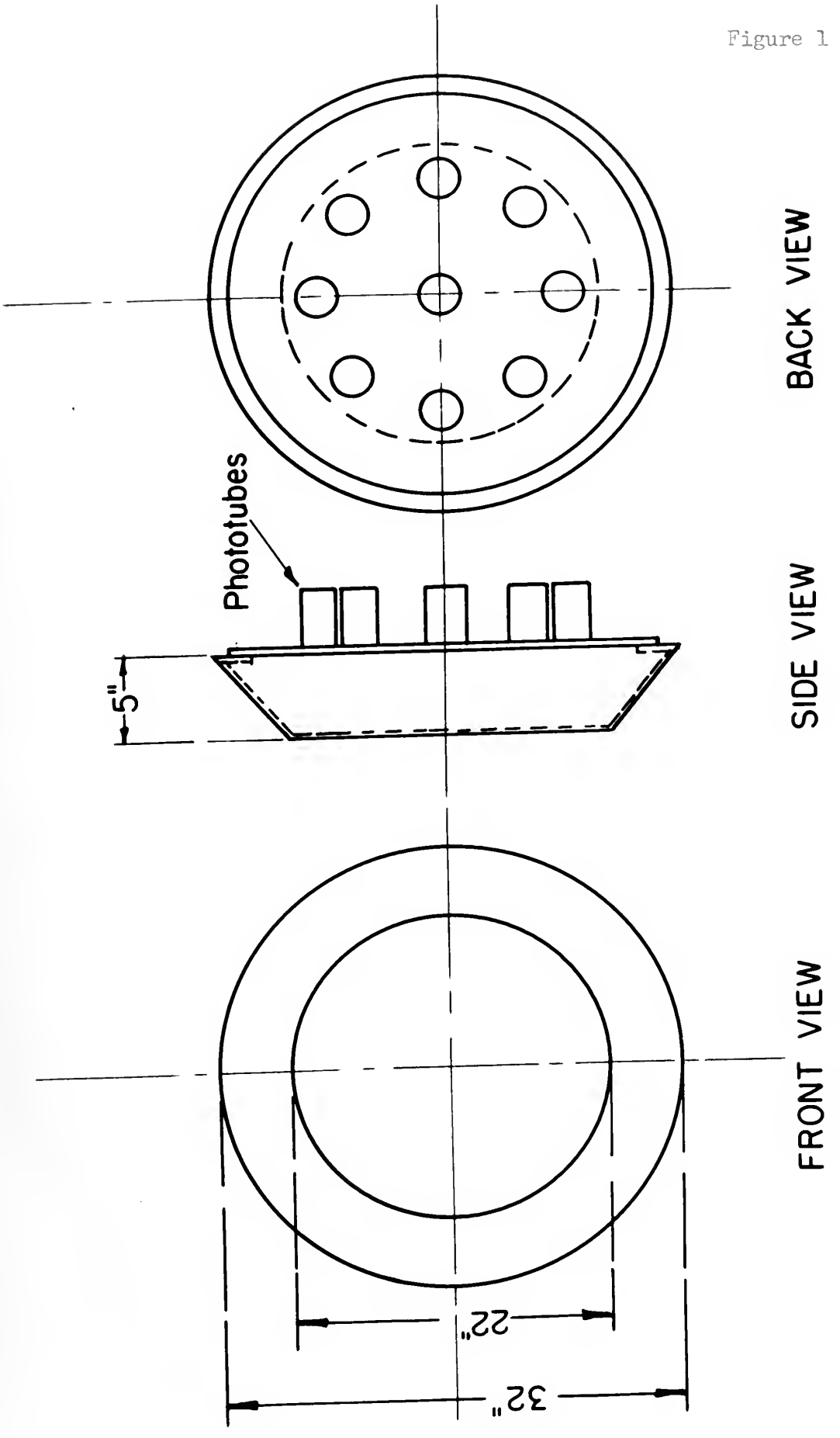

FLYING SAUCER NEUTRON COUNTER

Figure 2: Block Diagram of Electronics Circuit

An energy determination of the proton events required a coincidence between the front and back crystals of the proton counter. The output from the double coincidence circuit to scalers P_I and P_{II} recorded the number of proton events. The output from the triple coincidence circuit to scalers $(N+P)_I$ and $(N+P)_{II}$ recorded the number of n+p coincidences. The output from the triple coincidence circuit to scaler $N_{II}+p$ was a measure of the accidental n+p coincidences. The other scalers were employed to measure singles counting rates of the various components.

Figure 3: Block Diagram of Electronics Circuit

An energy detector on the proton events required a coincidence between the front and back crystals of the proton counter. The output from the double coincidence circuit to scalers P^{I} and P^{II} recorded the number of proton events. The output from the triple coincidence circuit to scalers $(N+P)^{I}$ and $(N+P)^{II}$ recorded the number of n+p coincidences. The output from the triple coincidence circuit to scaler $N^{II}+p$ was a measure of the accidental n+p coincidences. The other scalers were employed to measure singles counting rates of the various components.

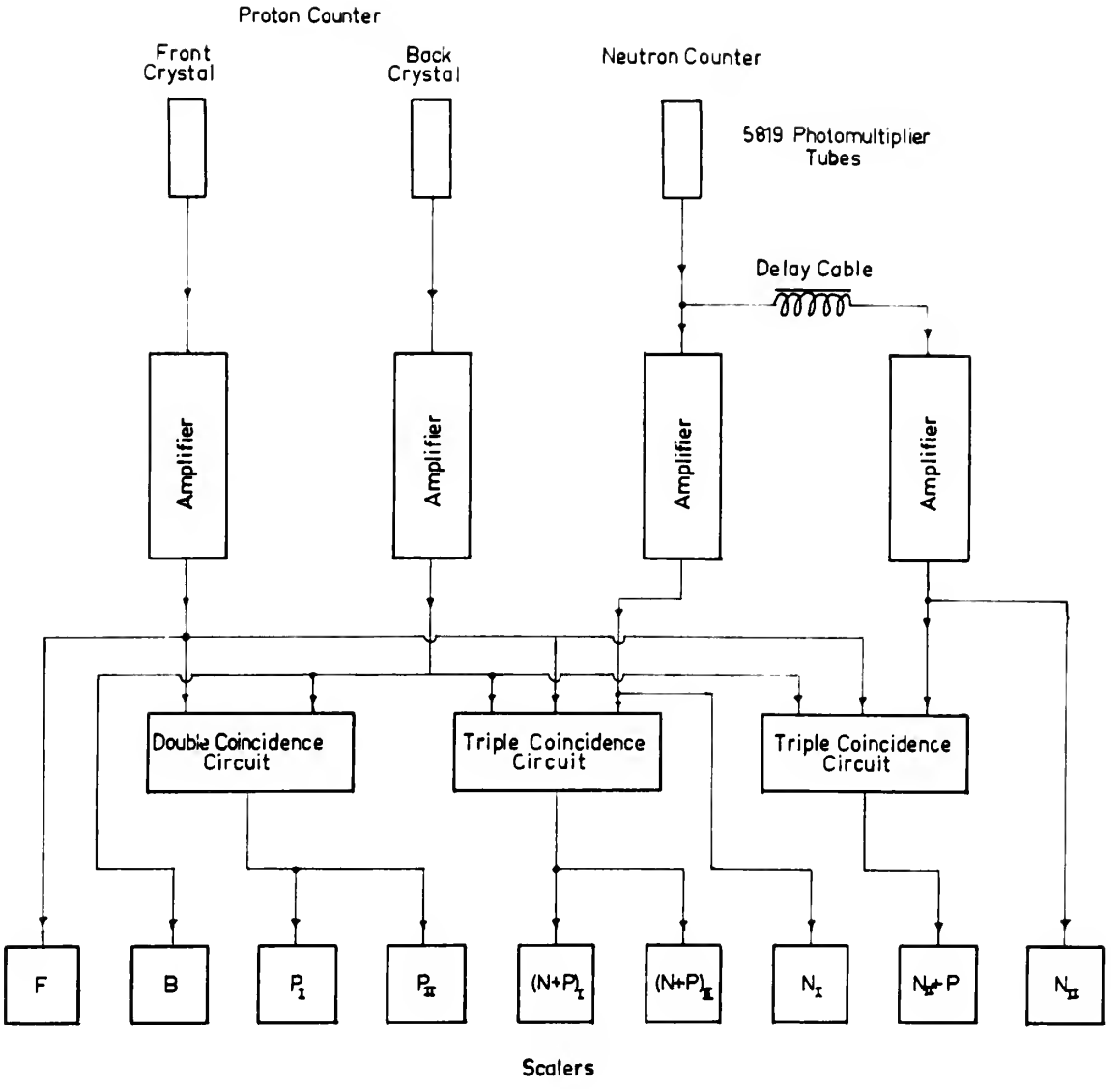
Proton Counter
Front Crystal
Back Crystal
Neutron Counter
5819 Photomultiplier Tubes
Delay Cable
Amplifier
Amplifier
Amplifier
Amplifier
Double Coincidence Circuit
Triple Coincidence Circuit
Triple Coincidence Circuit
F
B
P_I
P_{II}
$(N+P)_I$
$(N+P)_{II}$
N_I
$N_{II}+P$
N_{II}
Scalers

Figure 2

B. Calculations

1. Angular Resolution

In the calculations, it is assumed that the FS counter subtends a greater solid angle than does the beam of neutrons coming from the target as a result of the photodisintegration of the deuteron. Only those neutrons that are coincident with protons counted in the proton telescope are considered. As will be shown in the discussion concerning angular resolution of the small counter, this is a valid assumption in that the ratio of the solid angle subtended by the FS: solid angle of the beam is 1.56:1 for deuterium with the geometry employed. Therefore all of the neutrons coincident with protons counted enter the effective volume of the FS.

2. Calculated Efficiency of the FS Detector

a. Factors entering into efficiency

The efficiency of the FS detector is given by the following expression:

$$\text{Efficiency } (E_{bias}, E_n) \quad \frac{\sigma_{eff}(H) N_H + \sigma_{eff}(C) N_C}{\sigma_T(C) N_C + \sigma_T(H) N_H} \left(1 - e^{-\Sigma_t l_{eff}}\right)$$

where $\sigma_{eff}(H)$ = effective microscopic cross section for production of proton recoils from n-p scattering with energy $\geq E_{bias}$

$\sigma_{eff}(C)$ = effective microscopic cross section for production of observable charged particles from carbon nuclear events with E E_{bias}

N_C, N_H = number of atoms/cm^3 of carbon and hydrogen respectively

$\sigma_T(H)$, $\sigma_T(C)$ = total microscopic cross section of H and C respectively

Σ_t = reciprocal mean path = $\sigma_T(H) N_H + \sigma_T(C) N_C = \frac{1}{\lambda_T}$

l_{eff} = effective length of the counter

1

6. Calculations

1. Angular Resolution

In two orientations, it is apparent that the PS counter subtends a greater solid angle than does the beam of neutrons coming from the target as a result of the photodisintegration of the deuteron. Only those neutrons that are coincident with protons counted in the proton telescope are considered. As will be shown in the discussion concerning angular resolution of the small counter, this is a valid assumption in that the ratio of the solid angle subtended by the PS: solid angle of the beam is 1.56:1 for deuterium with the geometry employed. Therefore all of the neutrons coincident with protons counted enter the effective volume of the PS.

2. Calculated Efficiency of the PS Detector

a. Factors entering into efficiency

The efficiency of the PS detector is given by the following expression:

$$\text{Efficiency } (E_p^{bias}, E_n) \quad \frac{\sigma_1(C)\, N_C + \sigma_1(H)\, N_H}{\sigma_{eff}(H)\, N_H + \sigma_{eff}(C)\, N_C} \left(1 - e^{-\Sigma' l_{eff}}\right)$$

where $\sigma_{eff}(E)$ = effective microscopic cross section for production of proton recoils from n-p scattering with energy $\geq E_p^{bias}$

$\sigma_{eff}(C)$ = effective microscopic cross section for production of observable charged particles from carbon nuclear events with E_p^{bias}

N_C, N_H = number of atoms/cm^3 of carbon and hydrogen respectively

$\sigma_1(H)$, $\sigma_1(C)$ = total microscopic cross section of H and C respectively

Σ' = reciprocal mean path = $\sigma_1(H)\, N_H + \sigma_1(C)\, N_C = \frac{1}{\lambda_1}$

l_{eff} = effective length of the counter

The efficiency of the counter is a function of the neutron energy (E_n), bias energy (E_{bias}), cross section, and effective length of the counter. In addition to these factors, it is a function of a geometric factor dependent on the effective cross sectional area of the counter and the distribution of incident neutrons over this area. There will also be a reduction in counting efficiency due to attenuation of the neutron beam by any shielding material. An analysis of the individual factors effecting efficiency is given in the following paragraphs.

b. Effective Length, l_{eff}, and Wall Effects

In a counter of finite length, recoil protons originating near the back of the counter may strike the end of the counter before losing an observable amount of energy in the scintillator (i.e., Bias)*. Thus the effective length of the counter is the true length minus some average length for proton recoils to lose sufficient energy to produce a pulse larger than the bias setting. The loss of neutron counts due to the finite length of the counter is the same for both counters. It is a function of the bias applied to the neutron counter and the energy of the incident neutron. All biases are expressed in energy loss of an electron in the scintillator corresponding to the actual loss of the recoil protons. In view of the linear relationship between energy loss of an electron and pulse height this permits the use of a linear energy bias scale. Proton energy losses are converted to equivalent electron losses with the data of Birks.[17] The plots of

* Similarly, in a finite counter some proton recoils will strike the sidewalls of the counter before losing an amount of energy corresponding to the bias. It was not necessary to consider side losses in the calculations for the FS in view of the fact that the counter was much wider than the beam of incident neutrons.

(σ_n), pulse energy (bias), cross section, and effective length of the counter. In addition to these factors, it is a function of a geometric factor dependent on the effective cross sectional area of the counter and the distribution of incident neutrons over this area. There will also be a reduction in counting efficiency due to attenuation of the neutron beam by any shielding material. An analysis of the individual factors effecting efficiency is given in the following paragraphs.

b. Effective Length, l_{eff}, and Wall Effects

In a counter of finite length, recoil protons originating near the back of the counter may strike the end of the counter before losing an observable amount of energy in the scintillator (i.e., Bias)* Thus the effective length of the counter is the true length minus some average length for proton recoils to lose sufficient energy to produce a pulse larger than the bias setting. The loss of neutron counts due to the finite length of the counter is the same for both counters. It is a function of the bias applied to the neutron counter and the energy of the incident neutron. All biases are expressed in energy loss of an electron in the scintillator corresponding to the actual loss of the recoil protons. In view of the linear relationship between energy loss of an electron and pulse height this permits the use of a linear energy bias scale. Proton energy losses are converted to equivalent electron losses with the data of Birks. The plots of

* Similarly, in a finite counter some proton recoils will strike the sidewalls of the counter before losing an amount of energy corresponding to the bias. It was not necessary to consider side losses in the calculations for the 5" in view of the fact that the counter was much wider than the beam of incident neutrons.

electron pulse vs energy loss and proton pulse vs energy loss are assumed to be parallel above 15 Mev.

The procedure for estimating end losses was carried out graphically and is illustrated in figure 3. It consists of determining the energy of recoil protons as a function of proton laboratory angle through the relationship $E_p = E_n \cos^2\phi_{lab}$. (Figure 3a). The distance required for a proton of energy E_p to lose the bias energy, E_{bias}, is then determined from range-energy tables[29] and plotted as a function of proton recoil angle ϕ_{lab}. (Figure 3b). This is actually a three dimensional plot in that the surface which is formed by the ends of these vectors is a surface generated by the revolution of the curve about the $\phi_p = o$ axis. Lines are drawn on the plot perpendicular to the beam axis representing the end of the counter for n-p scattering at various distances from the counter end. The fraction of recoil protons of energy $\geq E_{bias}$ striking the end of the counter before losing E_{bias} is a function of ϕ counter and is given by $\frac{\int_0^{\phi_{counter}} \frac{d\sigma}{d\Omega}\, d\Omega}{\int_0^{\phi_{eff}} \frac{d\sigma}{d\Omega}\, d\Omega}$ where ϕ counter corresponds to the angle where the line representing the end of the counter and the curve of E_{bias} distance vs ϕ intersect. ϕ_{eff} is the proton angle at which the recoil proton energy $E_p = E_{bias}$. The values of $\frac{d\sigma}{d\Omega}$ for n-p scattering were obtained from Kelly et al[22] and were represented analytically by a function $\frac{d\sigma}{d\Omega} = A + B\cos^2\phi_{cm.}$ where $\phi_{cm.}$ is the scattering angle in the center of the mass coordinates. A plot of (probability of a neutron reaching a distance D without interacting) times (the probability of a

reaching a distance D without interacting) times (the probability of a
center of the mass coordinates. A plot of (probability of a neutron
a function $\frac{d\sigma}{d\Omega} = A + B\cos^2\phi_{cm}$. where ϕ is the scattering angle in the
were obtained from Kelly et al [22] and were represented analytically by
recoil proton energy $E_p = E_{bias}$. The values of $\frac{d\sigma}{d\Omega}$ for n-p scattering
E_{bias} distance vs ϕ intersect. ϕ_{eff} is the proton angle at which the
where the line representing the end of the counter and the curve of

$$\frac{\int_0^{\phi_{counter}} \frac{d\sigma}{d\Omega}\, d\Omega}{\int_0^{\phi_{eff}} \frac{d\sigma}{d\Omega}\, d\Omega}$$

where ϕ counter corresponds to the angle
before losing E_{bias} is a function of ϕ counter and is given by
of recoil protons of energy $\geq E_{bias}$ striking the end of the counter
n-p scattering at various distances from the counter end. The fraction
perpendicular to the beam axis representing the end of the counter for
the curve about the $\phi_p = 0$ axis. Lines are drawn on the plot per-
ends of these vectors is a surface generated by the revolution of
a three dimensional plot in that the surface which is formed by the
a function of proton recoil angle ϕ_{lab}. (Figure 3b). This is actually
E_{bias}, is then determined from range-energy tables [29] and plotted as
distance required for a proton of energy E_p to lose the bias energy.
angle through the relationship $E_p = E_n \cos^2\phi_{lab}$. (Figure 3a). The
the energy of recoil protons as a function of proton laboratory
ically and is illustrated in figure 3. In counts of determining

The procedure for obtaining the losses was carried out graph-

removed by the 1/2 inch above 1/2 inch.

Figure 3: End Losses

Figure 3a is a plot of recoil proton energy as a function of recoil proton angle for n-p scattering by 130 Mev neutrons.

For each recoil proton energy, the distance required for the proton to lose the bias energy, E_{bias}, is determined from range-energy tables. A plot of this distance, also as a function of proton recoil angle, is shown in figure 3b. For a hypothetical "counter wall" at various distances, x, from an n-p scattering event, the fraction of effective protons ($E_p \geq E_{bias}$) that strike the "counter wall" before losing E_{bias} is calculated.

Figure 3: Lead losses

Figure 3a is a plot of recoil proton energy as a function of recoil proton angle for n-p scattering by 130 Mev neutrons.

For each recoil proton energy, the distance required for the proton to lose the bias energy, E_{bias}, is determined from range-energy tables. A plot of this distance, also as a function of proton recoil angle, is shown in figure 3b. For a hypothetical "counter wall" at various distances, x, from an n-p scattering event, the fraction of effective protons ($E_p \geq E_{bias}$) that strike the "counter wall" before losing E_{bias} is calculated.

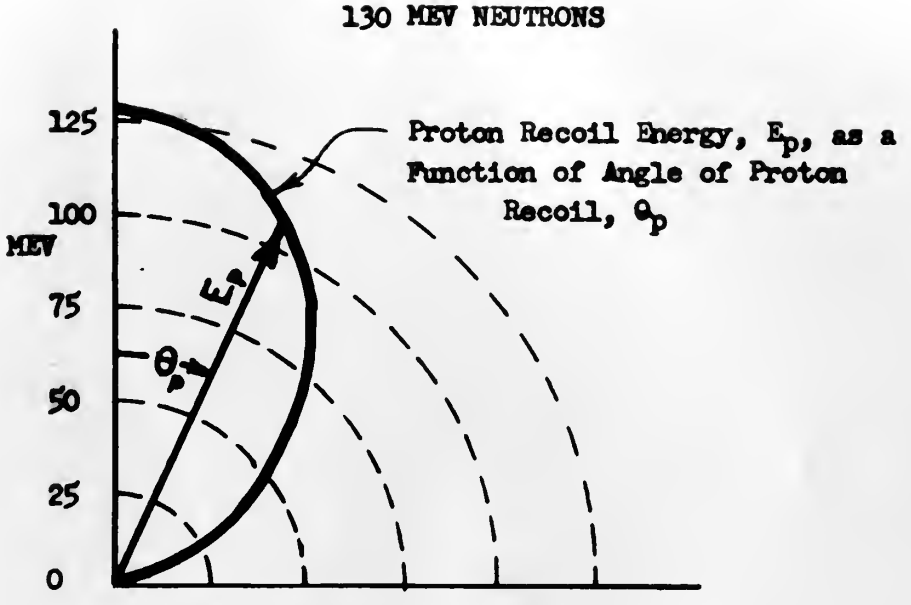

Figure (3a)

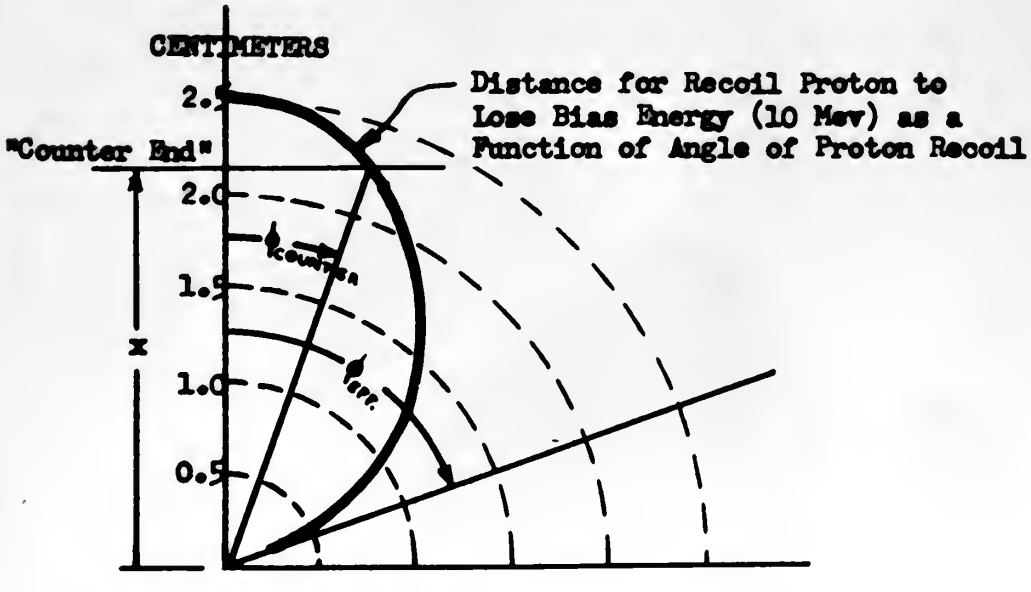

Figure (3b)

recoil proton losing E_{bias} in the counter without striking the counter end if it originated at D) versus distance in the counter was made, figure 4. The point l_{eff} at which the probability areas on the graph of figure 4 were equal was taken as the effective end of the counter. l_{eff} is shown on the graph.

The values of $\frac{d\sigma}{d\Omega}$ and this whole calculation are for pure n-p scattering. The contribution of energetic protons and deuterons from the carbon is considerable [20,21] and is taken into account in the calculations (see below). Neglecting the carbon in the calculation of wall losses introduces no appreciable errors in that the carbon contribution is predominantly at lower energies. Any error that is introduced is on the conservative side, that is slightly overestimating the end losses.

c. Carbon Contribution

The contribution of energetic charged particles produced by high energy neutrons interacting with the carbon nuclei present is appreciable. Kellogg has investigated the Cross Sections for Products of 90 Mev Neutrons on Carbon [20] and results pertinent to this study are given in tabular form below:

σ	VALUE (milli-barns) 90 Mev Neutrons		
Carbon, Total	504 ± 80		
Carbon: production of protons with	$E_p > 0$ 173 ± 15	$E_p > 20$ Mev 85.3 ± 9.2	$E_p > 35$ Mev 57.5 ± 5.
Carbon: production of deuterons with	$E_d > 0$ 90 ± 10	$E_d > 27$ Mev 26.1 ± 3.4	
Hydrogen, Total	77 ± 1.5		

90 Mev Neutrons on Carbon and results pertinent to this study are given in tabular form below:

C	VALUE (milli-barns) 90 Mev Neutrons		
Carbon, Total	501 ± 80		
Carbon: production of protons with	$E_p > 0$ 173 ± 15	$E_p > 20$ Mev 85.3 ± 9.2	$E_p > 35$ Mev 57.5 ± 5.
Carbon: production of deuterons with	$E_d > 0$ 90 ± 10	$E_d > 27$ Mev 26.1 ± 3.4	
Hydrogen, Total	77 ± 1.5		

Figure 4: l_{eff}, Effective Length of the Counter

A plot of P vs distance into the counter, D. P is defined as (probability of a neutron reaching a distance D in the counter) times (probability that a recoil proton, $E_p \geqslant E_{bias}$, will produce a light pulse $\geqslant$bias before striking the counter wall). The values of P plotted are for 130 Mev neutrons, 10 Mev bias. l_{eff} is shown for a 10 Mev bias where the two shaded probability areas are equal. The value of l_{eff} for a 20 and 45 Mev bias is shown for both counters.

Figure 11. l_{eff}, Effective Length of the Counter

A plot of P vs distance into the counter, D. P is defined as (probability of a neutron reacting a distance D in the counter) times (probability that a recoil proton, $E_p \geq E_{bias}$, will produce a light pulse $\geq$bias before striking the counter wall). The values of P plotted are for 150 Mev neutrons, 10 Mev bias. l_{eff} is shown for a 10 Mev bias where the two shaded probability areas are equal. The value of l_{eff} for a 20 and 45 Mev bias is shown for both counters.

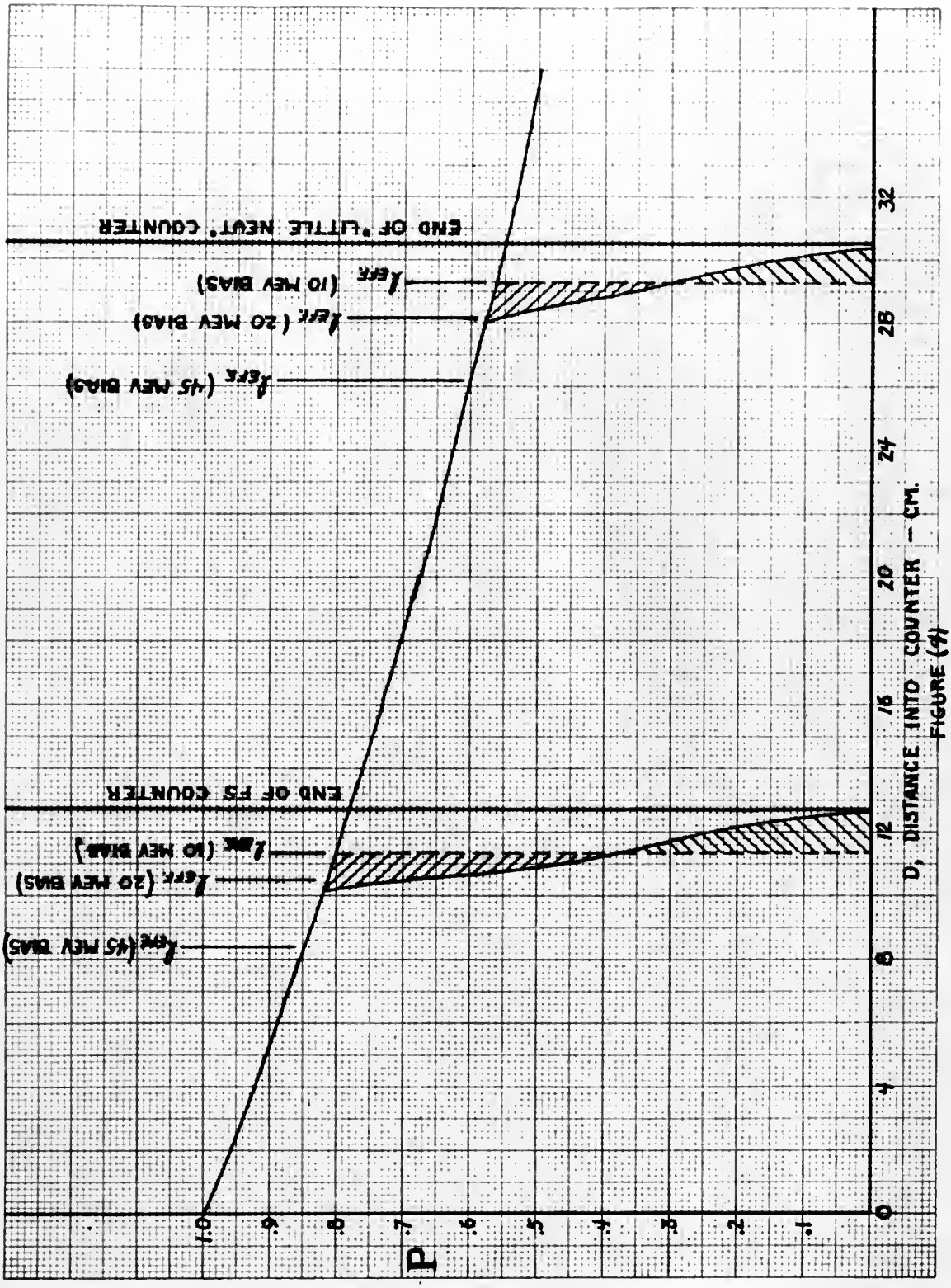
P
1.0
.9
.8
.7
.6
.5
.4
.3
.2
.1
0
4
8
12
16
20
24
28
32
D, DISTANCE INTO COUNTER — CM.
END OF FS COUNTER
END OF "LITTLE NEUT" COUNTER
(45 MEV BIAS)
(20 MEV BIAS)
(10 MEV BIAS)

FIGURE (4)

In view of the non-availability of such cross sections at other high energies, the cross sections for production of energetic charged particles from carbon were assumed to be proportional to the total cross section, with appropriate considerations of the energy scale of the charged particles. The total cross section for carbon at several high energies has been measured by Taylor and Wood.[7]

d. Results of Calculations of FS Efficiency

A plot of calculated FS efficiency vs E_{bias} at $E_n = 130$ Mev is given in figure 5. The calculated values of efficiency vs neutron energy are given in Table 1.

Since the counter was shielded by 3" of lead, the neutron beam would be attenuated to $e^{-\Sigma_t(Pb)3"}$ before reaching the counter if all interactions in the lead removed neutrons from the beam. However this is not the case; some neutrons are scattered back into the counter, figure 5 includes one curve for total lead attenuation and one curve for no lead in front of the counter. The effect of the lead is discussed further in the next section.

C. Experimental Investigation

The apparatus was set up as described earlier and shown in figure 6. A D_2O-H_2O subtraction of n+p coincidences was made to determine the efficiency and characteristics of the FS by use of the photodisintegration of deuterium. Accidentals were subtracted as described previously. From kinematic relations the energy of the neutrons being detected was known to a small relative energy width, $\pm$ 12.5 Mev. The response of the FS was determined to be uniform over its face by use

response of the BS was determined to be uniform over its face by use detected was known to a small relative energy width, ± 1%. The of the BS by use of the photodisintegration of deuterium. Accidentals were subtracted as described previously. From kinematic relations the energy of the neutrons being the efficiency and characterization of the D_2O-H_2O substraction of n-p coincidences was made to determine figure 6. A

c. Experimental Investigation

The apparatus was set up as described earlier and shown in figure 5 included one curve for total lead attenuation and one curve for no lead in front of the counter. The effect of the lead is discussed further in the next section.

In this case some neutrons are scattered back into the counter, interactions in the lead removed neutrons from the beam. However would be attenuated to $e^{-\Sigma_f(Pb)3"}$ before reaching the counter if all

Since the counter was shielded by 3" of lead, the neutron beam energy are given in Table I.

given in figure 5. The calculated values of efficiency vs neutron A plot of calculated BS efficiency vs E_{beta} at $E_n = 1.30$ Mev is

d. Results of Calculations of BS Efficiency

high energies has been measured by Taylor and Wood.[7]

the charged particles. The total cross section for carbon at several cross section, with corrections considerations of the energy needs of

Figure 5: Flying Saucer Counter Efficiency vs Bias

The experimental values are for 129 ± 12.5 Mev neutrons. The calculated values for 130 Mev neutrons are shown in the two curves. The upper curve is the expected value if there were no attenuation of the neutron beam in the lead shield. The other curve assumes that all neutron interactions with the lead remove neutrons from the beam.

Figure 3: Fission source fraction efficiency vs Pbaa

The experimental values are for 129 ± 12.5 Mev neutrons. The calculated values for 130 Mev neutrons are shown in the two curves. The upper curve is the expected value if there were no attenuation of the neutron beam in the lead shield. The other curve assumes that all neutron interactions with the lead remove neutrons from the beam.

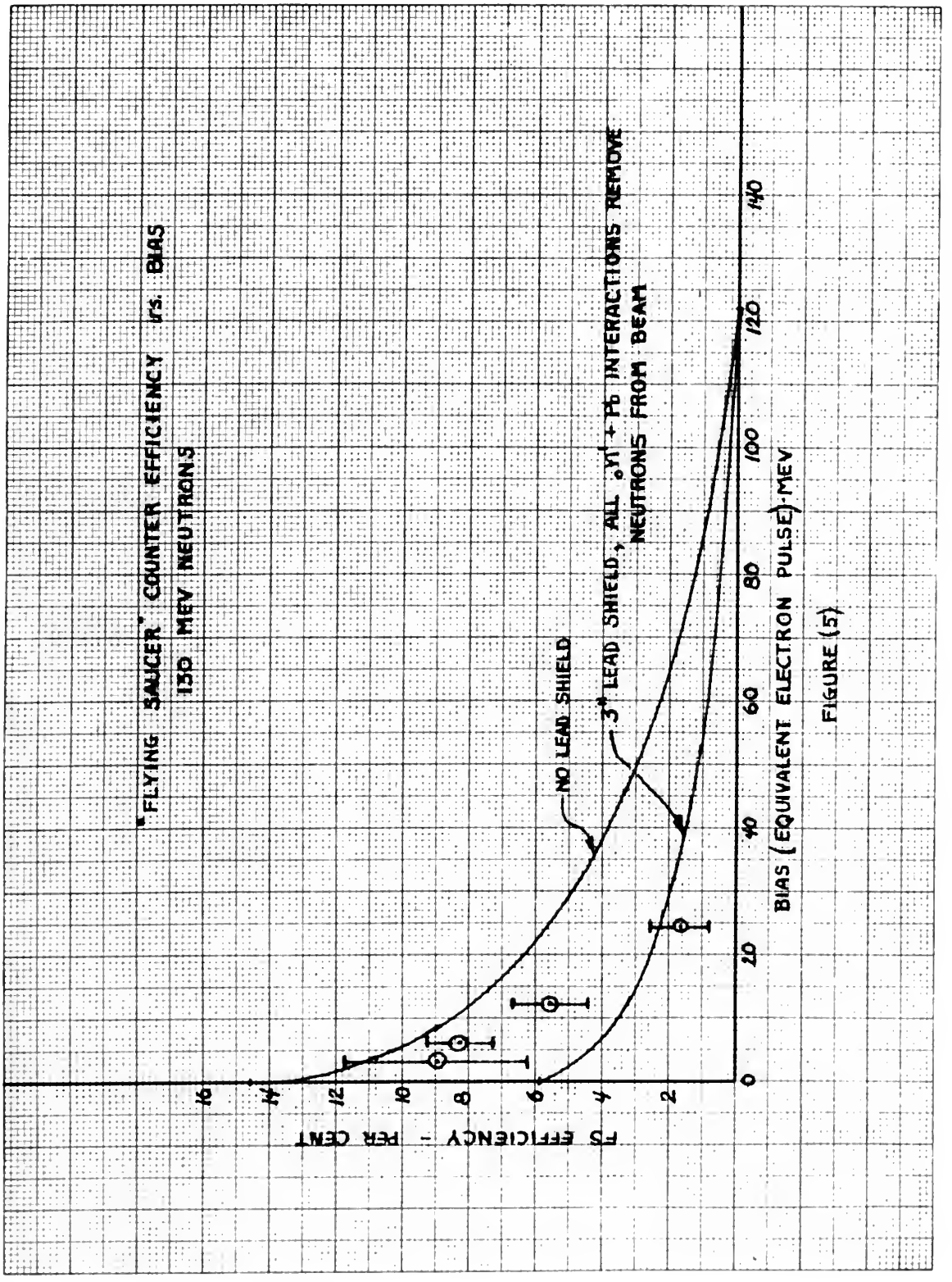
"FLYING SAUCER" COUNTER EFFICIENCY vrs. BIAS
150 MEV NEUTRONS
NO LEAD SHIELD
3" LEAD SHIELD, ALL π^0 + Pb INTERACTIONS REMOVE NEUTRONS FROM BEAM
FS EFFICIENCY - PER CENT
BIAS (EQUIVALENT ELECTRON PULSE)-MEV
0
20
40
60
80
100
120
140
2
4
6
8
10
12
14
16

FIGURE (5)

Figure 6: Geometry employed in experiments with Flying Saucer Neutron Counter

Figure 61: Geometry employed in experiments with Flying Saucer Neutron Counter

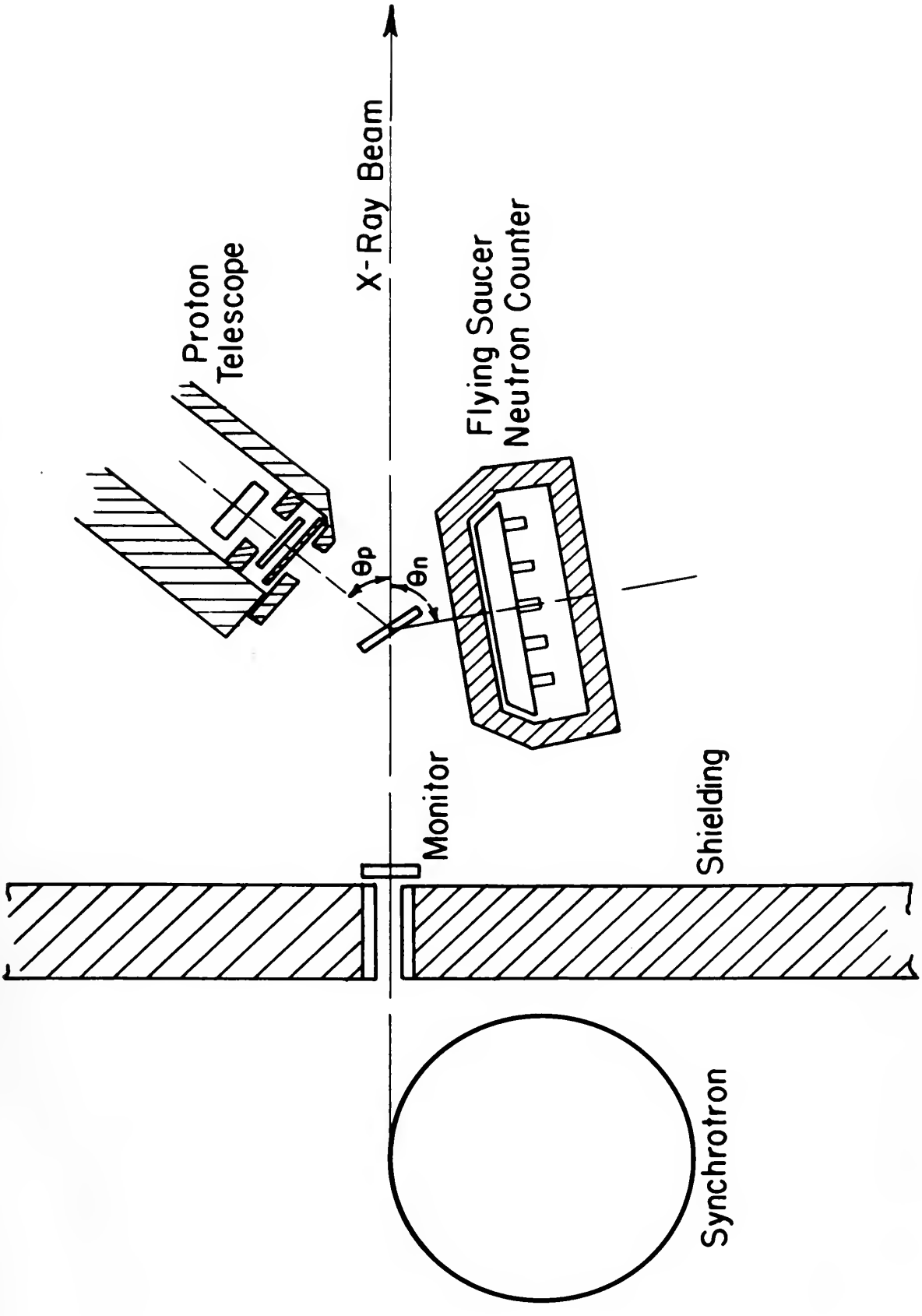
X-Ray Beam
Proton Telescope
Flying Saucer Neutron Counter
θ_p
θ_n
Monitor
Shielding
Synchrotron

Figure 6

of a small radium source. The bias of the FS was determined absolutely by a radium γ cut off. In view of the linear relation between electron pulse height and energy loss, this value could be extrapolated to our operating point which corresponded to a 6.1 Mev electron bias. The data taken on FS yielded the following information:

a. Efficiency of FS vs E_{bias} (E_γ = 260 Mev; E_n = 129 Mev) compared with calculated values in figure 5.

b. Effect of distance of FS from target vs counting rate of n+p from lithium and oxygen (H_2O). Figure 7.

c. Efficiency of FS vs E_n (E_γ = 260, 200 Mev; E_{bias} = 6.1 Mev). See table 1, page 19.

D. Discussion of Results

1. Efficiency of FS vs E_{bias}; E_n = constant = 129 Mev

Figure 5 shows clearly the correspondence between the calculated and experimental values for efficiency. The deviation from the calculated values is attributed to contributions from the lead shield. As is shown, practically all the neutrons that interact with the lead arrive in the counter volume as energy degraded neutrons. Hence at low bias there is probably no appreciable loss of counts due to lead attenuation; however, as the bias voltage is increased, the lower energy neutrons scattered from the lead are cut out rapidly and the experimental curve approaches the calculated curve representing completely effective lead attenuation.

-ute-

by a width γ cut off. In view of the linear relation between

-ute-

pulse height and energy loss, this value could be extra-

polated to our operating point which corresponded to a 6.1 Mev

electron bias. The data taken on PS yielded the following infor-

mation:

a. Efficiency of PS vs E_{bias} (E_γ = 260 Mev; E_n = 129 Mev) com-

pared with calculated values in Figure 5.

b. Effect of distance of PS from target vs counting rate of n+p

from lithium and oxygen (Li_2O). Figure 7.

c. Efficiency of PS vs E_n (E_γ = 260, 200 Mev; E_{bias}=6.1 Mev).

See table I, page 19.

D. Discussion of Results

1. Efficiency of PS vs E_{bias}; E_n = constant = 129 Mev

Figure 5 shows clearly the correspondence between the cal-

culated and experimental values for efficiency. The deviation from

the calculated values is attributed to contributions from the lead

shield. As is shown, practically all the neutrons that interact with

the lead arrive in the counter volume as energy degraded neutrons.

Hence at low bias there is probably no appreciable loss of counts due

to lead attenuation; however, as the bias voltage is increased, the

lower energy neutrons scattered from the lead are cut out rapidly and

the experimental curve approaches the calculated curve representing

completely effective lead attenuation.

Figure 7: Ratio of $\frac{n+p}{p}$ Counting Rates from Li and O as a function of FS Distance from Target

The ratio of n+p coincidences to proton counts is shown as a function of FS distance from target. The distance scale is in solid angle subtended by the FS at the center of the target. The actual distances in inches are noted above the solid angle coordinate.

The predicted distance at which the ratio should fall to half the plateau value is shown on the graph as $O(\frac{1}{2})$ and $Li(\frac{1}{2})$.

In both cases $E_n = E_p = 129$ Mev $\quad E_{bias} = 6.1$ Mev

Figure 1: Ratio of $\frac{\pi^+p}{p}$ scattering versus T_{π^+} LH and C as a function of TS distance from Target

The ratio of π^+p coincidences to proton counts is shown as a function of TS distance from target. The distance scale is an solid angle subtended by the TS at the center of the target. The actual distances in inches are noted above the solid angle coordinate.

The predicted distance at which the ratio should fall to half the plateau value is shown on the graph as $0(\frac{1}{2})$ and $1(\frac{1}{2})$.

In both cases $E^{\pi} = E^{p} = 129$ Mev $E^{bias} = 6.1$ Mev

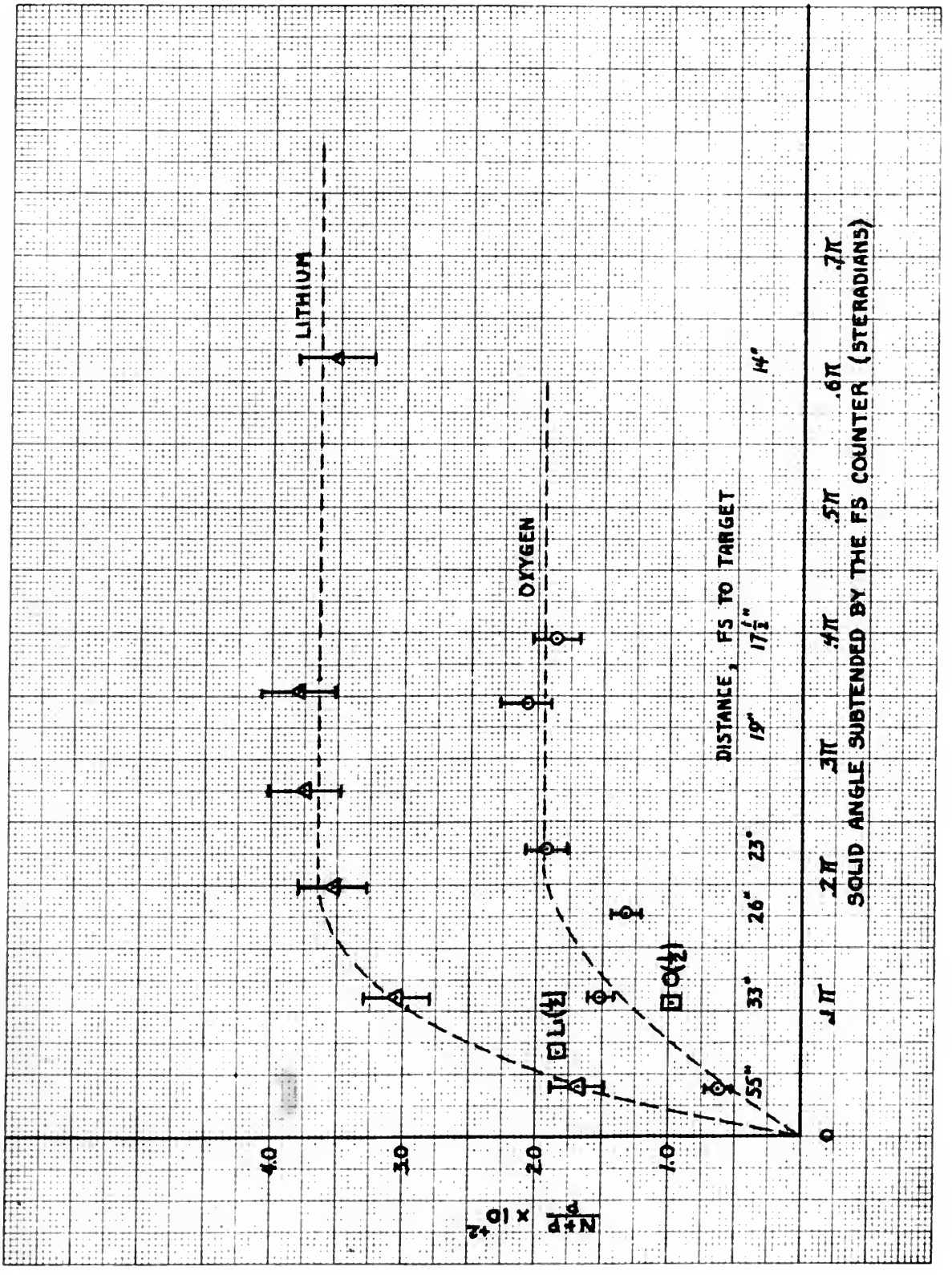
LITHIUM
OXYGEN
Li(½)
O(½)
4.0
3.0
2.0
1.0
0
$\frac{N^+P}{P} \times 10^{-2}$
DISTANCE, FS TO TARGET
55"
33°
26"
23°
19"
17½"
14"
π
2π
3π
4π
5π
6π
7π
SOLID ANGLE SUBTENDED BY THE FS COUNTER (STERADIANS)

Figure 7

2. Effect of FS Distance from Target on n p from lithium and oxygen

A plot of n p coincidences vs FS distance from target is given in figure 7. This plot shows the effectiveness of the large solid angle coverage by the FS. The solid angle subtended by the median plane of the counter at the target center is shown as absissa underneath the distance scales. The angular distribution of the coincident neutrons from Li and O was determined with the small counter, see H. Wilson's thesis.[30] From these curves we would expect the counting rate with the FS counter to have the gross features shown in figure 7, namely a plateau at large solid angles and a fall off starting when the solid angle no longer contains the entire neutron distribution. One can try to be quantitative by comparing the value at which the FS counter should count one half of its plateau counting rate with the width obtained on the small counter. Such a comparison requires a knowledge of the curve shape. A theory for the curve shape has been proposed by Wattenberg.[31] A fairly good quantitative check is obtained by assuming the curve is a Gaussian which should be weighted by the solid angle. The predicted half value points are indicated in figure 7. Their agreement with the experimental values is considered satisfactory in view of the assumption being made. The plateau of the lithium curve extends to greater FS distances than the oxygen plateau. This is a confirmation of the values obtained for the angular half widths with the small counter, see reference 30.

3. Efficiency of FS vs Neutron Energy

Table 1 shows the correlation between the calculated and experimental values of FS efficiency as a function of neutron energy.

3. Efficiency of Ts vs Neutron Energy

Table I shows the correlation between the calculated and experimental values of Ts efficiency as a function of neutron energy.

The increase of efficiency with increasing neutron energy can be attributed in part to the effects of the 3" of lead shielding the FS. The cross section for neutron interactions with lead (above resonances) is flat out to approximately 90 Mev.[6] It falls in the energy interval from ~90 to 140 Mev where it again becomes flat. This effect tends to cancel out the lowering of efficiency due to the decrease in cross section for production of energetic charged particles in the scintillator at higher energies.

At neutron energies of 70 and 78 Mev the experimental value of efficiency approaches that value obtained for the lead being completely effective in removing neutrons from the beam. At the higher neutron energies, 129 and 171, it approaches the value calculated for no lead attenuation.

A further factor leading to an increasing efficiency with increasing neutron energy is the effect of the carbon nuclei present in the scintillator. The cross section for the ejection of energetic charged particles from the carbon nuclei by fast neutrons is a greater fraction of the total cross section at higher energies.

TABLE 1 Efficiency of FS Counter as a Function of Neutron Energy
Neutron Bias 6.1 Mev

E_x Mev	$E_{neutron}$ Mev	Experimental Efficiency % *	Calculated Efficiency--%	
			3" Pb Shield**	No Pb Shield
200	70	5.79 ± .75	4.10	13.2
260	78	5.46 ± .50	3.41	11.0
200	99	7.8 ± .87	3.43	10.1
260	99	6.49 ± .56	3.43	10.1
260	129	8.14 ± .50	4.10	9.7
260	171.6	8.15 ± .93	3.97	8.05

* Defined as $\frac{n+p}{p}$ from deuterium

** All Pb interactions assumed to remove neutrons from beam.

TABLE I Efficiency of PB Counter as a Function of Neutron Energy
Neutron Bias 6.1 Mev

E_n Mev	Neutron Mev	Experimental Efficiency % *	Calculated Efficiency--%	
			3" Pb Shield**	No Pb Shield
200	70	5.79 ± .75	6.10	13.2
260	78	5.46 ± .50	3.41	11.0
200	99	7.8 ± .87	3.43	10.1
260	99	6.49 ± .56	3.43	10.1
260	129	8.14 ± .50	6.10	9.7
260	172.6	8.15 ± .93	3.97	8.05

* Defined as $\frac{n+p}{p}$ from deuterium

** All Pb interactions assumed to remove neutrons from beam.

IV. STUDY OF SMALL, "LITTLE NEUT", NEUTRON DETECTOR

A. Description of "little neut"

"Little neut" was constructed of clear plastic in the shape of a cylinder 12" long by 4" in diameter (see figure 8). Light from the scintillating liquid was funneled to the photosensitive face of a single RCA 5819 phototube by a small truncated cone of lucite. The lucite was in optical contact with the end of the counter and the face of the phototube.

"Little neut" was shielded from background radiation by 2" of lead in front of the detector and a cylindrical lead house 1 1/8" thick surrounding the counter. "Little neut" was filled with the same liquid scintillator as the FS with the exception that no "Popop" was added. This decreased the response time of the scintillator by a factor of ~8; however the pulses obtained were smaller in magnitude. The physical properties of the scintillator remained identical with those of the FS.

Accidental n+p coincidences were handled in the same manner as with the FS.

B. Calculations

1. Angular Resolution

a. Finite width of the counter, side wall losses

Some of the neutrons entering the counter will produce energetic charged particles near the side walls of the counter. A fraction of the charged particles so produced will strike the side walls of the counter before travelling far enough to lose an energy corresponding

IV. Design of Small "Little Rest" Neutron Detector

A. Description of "Little Rest"

"Little Rest" was constructed of clear plastic in the shape of a cylinder 12" long by 5" in diameter (see figure 8). Light from the scintillating liquid was funneled to the photosensitive face of a single 6CA 5819 phototube by a small truncated cone of lucite. The lucite was in optical contact with the end of the counter and the face of the phototube.

"Little Rest" was shielded from background radiation by 2" of lead in front of the detector and a cylindrical lead house 1 1/8" thick surrounding the counter. "Little Rest" was filled with the same liquid scintillator as the P5 with the exception that no "Popop" was added. This decreased the response time of the scintillator by a factor of ~8; however the pulses obtained were smaller in magnitude. The physical properties of the scintillator remained identical with those of the P5.

Accidental n-p coincidences were handled in the same manner as with the P5.

B. Calculations

1. Angular Resolution

a. Finite width of the counter, side wall losses

Some of the neutrons entering the counter will produce energetic charged particles near the side walls of the counter. A fraction of the charged particles so produced will strike the side walls of the counter before traveling far enough to lose an energy corresponding

Figure 8: Small Neutron Counter, "Little Neut".

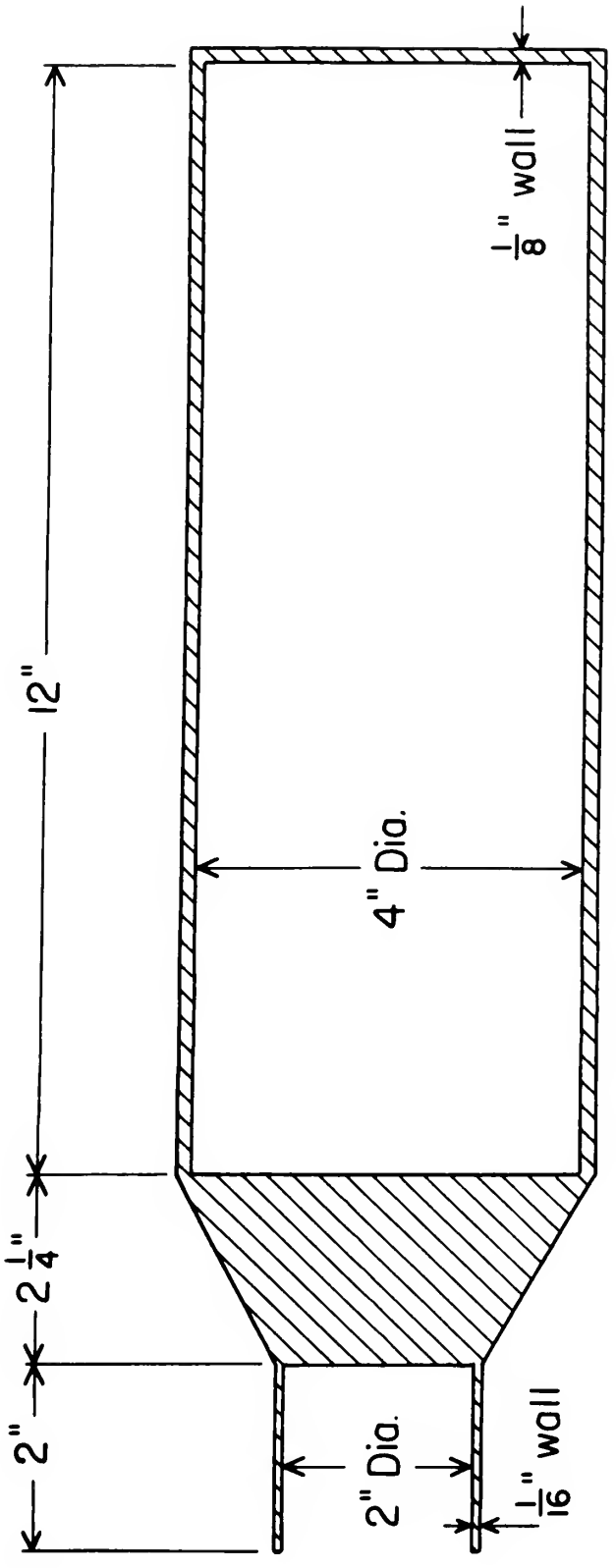

Figure 8

to the bias. Some criteria must be established to estimate the effective volume of the counter which is lost due to these events. This calculation is illustrated graphically in figure 9 and is similar in many respects to the calculation of end effects in the FS. The wall of the counter was approximated by a plane. The criteria established was as follows: That distance, x, from the counter wall can be assumed ineffective where 50% of the recoil protons from n-p scattering that scatter to one side of the median plane will strike the wall of the counter before losing an energy corresponding to a given bias. Therefore the effective radius of the counter is equal to $R_{counter}(2")$ minus x. Where x is a function of bias and neutron energy. Disregarding the carbon contribution here (as is discussed for end effect of FS) results in slightly overestimating the volume of the counter lost due to side wall effects. For 130 Mev neutrons and 10 Mev bias, x is 0.4 cm.

b. Effect of Finite Width Target and Target Angle

(1) Statement of problem

Since the deuterons that undergo photodisintegration are at rest initially in the laboratory, the neutron-proton pairs arising will be ejected back to back in the center of mass coordinates. Thus, for a given γ ray, the angle of the neutron is determined if the angle at which the proton is ejected is known. The proton detector is well defined spatially and the energy spread of protons accepted leads to a very small deviation from the angle between the neutron and proton of the pair corresponding to the median energy proton accepted. It is

of the pair corresponding to the median energy proton accepted. It is a very small deviation from the angle between the neutron and proton defined spatially and the energy spread of protons accepted leads to at which the proton is ejected is known. The proton detector is well for a given γ ray, the angle of the neutron is determined if the angle will be ejected back to back in the center of mass coordinates. Thus, at rest initially in the laboratory, the neutron-proton pairs arising

Since the deuterons that undergo photodisintegration are at

(1) Statement of problem

b. Effect of Finite Width Target and Target Angle

and 10 Mev bias, x is 0.4 cm.

of the counter lost due to side wall effects. For 130 Mev neutrons for end effect of W5) results in slightly overestimating the volume energy. Disregarding the carbon contribution here (as is discussed to $P_{counter}(2")$ minus x. Where x is a function of bias and neutron given bias. Therefore the effective radius of the counter is equal the wall of the counter before losing an energy corresponding to a scattering that scatter to one side of the median plane will strike be assumed ineffective where 50% of the recoil protons from n-p

liahed was as follows: That distance, x, from the counter wall can wall of the counter was approximated by a plane. The criteria estab- in many respects to the calculation of end effects in the W5. The

This calculation is illustrated graphically in figure 9 and is similar

efficiency volume of the counter which is lost due to these events.

Figure 9: Side Wall Losses

Side wall losses are treated in a manner similar to the end losses. A plot of distance for a recoil proton to lose the bias energy (10Mev) vs proton recoil angle is made for E neutron = 130 Mev. (Figure 9a). Our plot need only be in two dimensions since the locus of these points is symmetric about the axis of the neutron beam. A set of parallel lines are drawn parallel to the wall of the counter. Two are shown in the figure at distances A and A' from the beam axis. The fraction of effective recoil protons losing E_{bias} between these lines is

$$f_{AA'} = \frac{\int_{\phi_1}^{\phi_2} \frac{d\sigma}{d\Omega} d\Omega + \int_{\phi_3}^{\phi_4} \frac{d\sigma}{d\Omega} d\Omega}{\int_{\phi=0}^{\phi_{eff}} \frac{d\sigma}{d\Omega} d\Omega}$$

where $\frac{d\sigma}{d\Omega}$ is for n-p scattering

$\phi = \phi_{eff}$ when $E_p = E_{bias}$

This fraction is spread uniformly about the beam axis. Looking down the beam axis in figure 3b, the counter wall is positioned by trial and error. With the counter wall at x, the fraction of $f_{AA'}$ striking the wall before losing E_{bias} is $\frac{\psi}{2\pi}$. The loss of counter radius is given by that value of x for which $\frac{1}{2\pi} \sum_i (f_{AA'})_i \psi_i = .25$

Where the summation is over all the segments cut by the parallel lines.

parallel lines.

Where the summation is over all the segments cut by the

of x for which $\frac{1}{2\pi}\sum (t_{AA'})_i \Phi_i$ = .25 + .

is $\frac{\Phi}{2\pi}$. The loss of counter reading is given by that value

the fraction of $f_{AA'}$ striking the wall before losing E_p^{bias}

positioned by trial and error. With the counter wall at x,

looking down the beam axis in figure 3b, the counter wall is

This fraction is spread uniformly about the beam axis.

$\phi = \phi_{eff}$ when $E_p = E_p^{bias}$

$$f_{AA'} = \frac{\int_{\phi_1}^{\phi_2} \frac{d\sigma}{d\Omega}\, d\Omega + \int_{\phi_3}^{\phi_4} \frac{d\sigma}{d\Omega}\, d\Omega}{\int_{\phi=0}^{\phi=\phi_{eff}} \frac{d\sigma}{d\Omega}\, d\Omega}$$ where $\frac{d\sigma}{d\Omega}$ is for n-p scattering

protons losing E_p^{bias} between these lines is

A' from the beam axis. The fraction of effective recoil

counter. Two are shown in the figure at distances A and

parallel lines are drawn parallel to the wall of the

symmetric about the axis of the neutron beam. A set of

be in two dimensions since the locus of these points is

for E neutron = 130 Mev. (Figure 9a). Our plot need only

Use the big energy (10Mev) proton recoil angle is made

the locus. Plot of distance for a recoil proton in

130 MEV NEUTRONS

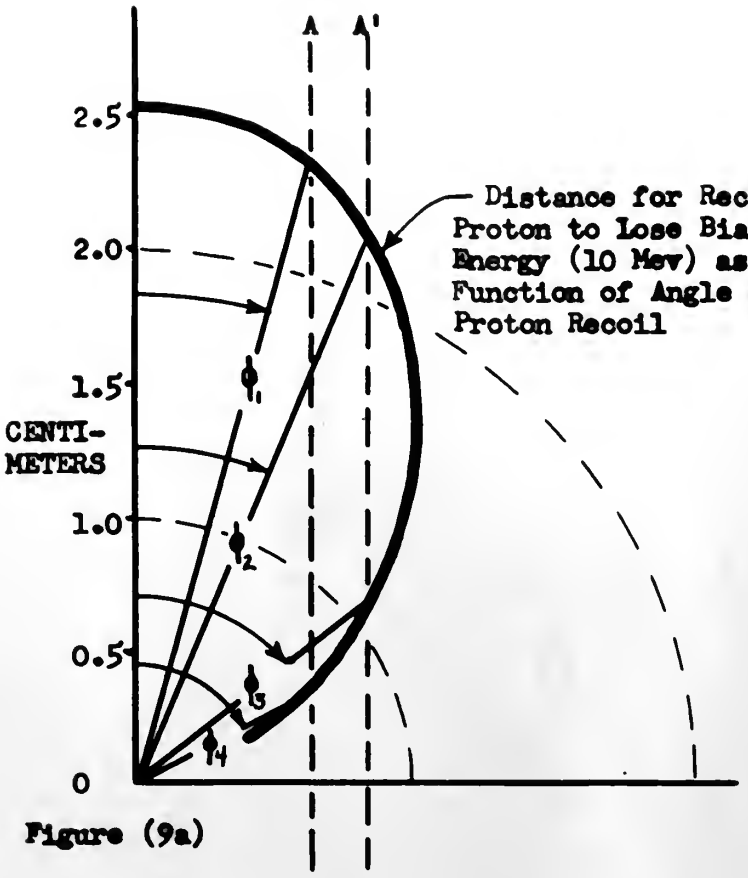

Figure (9a)

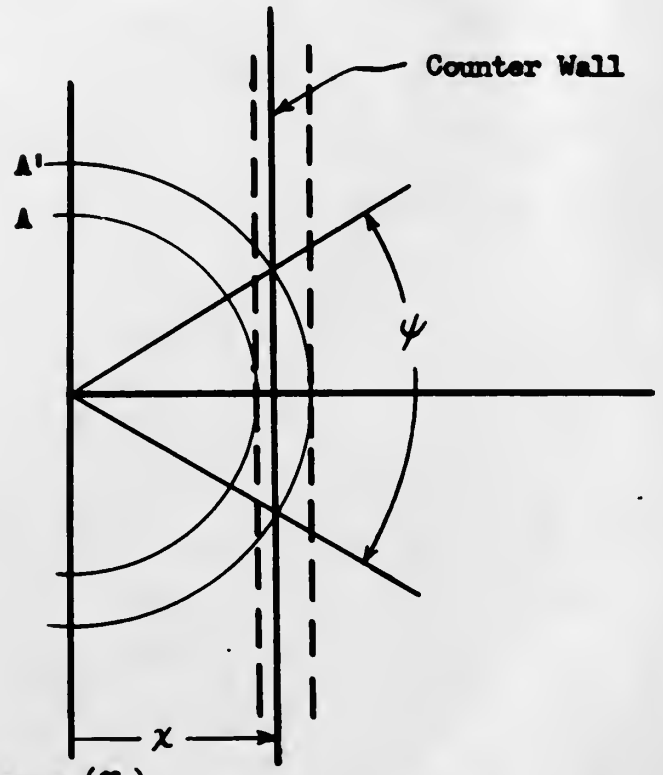

Figure (9b)

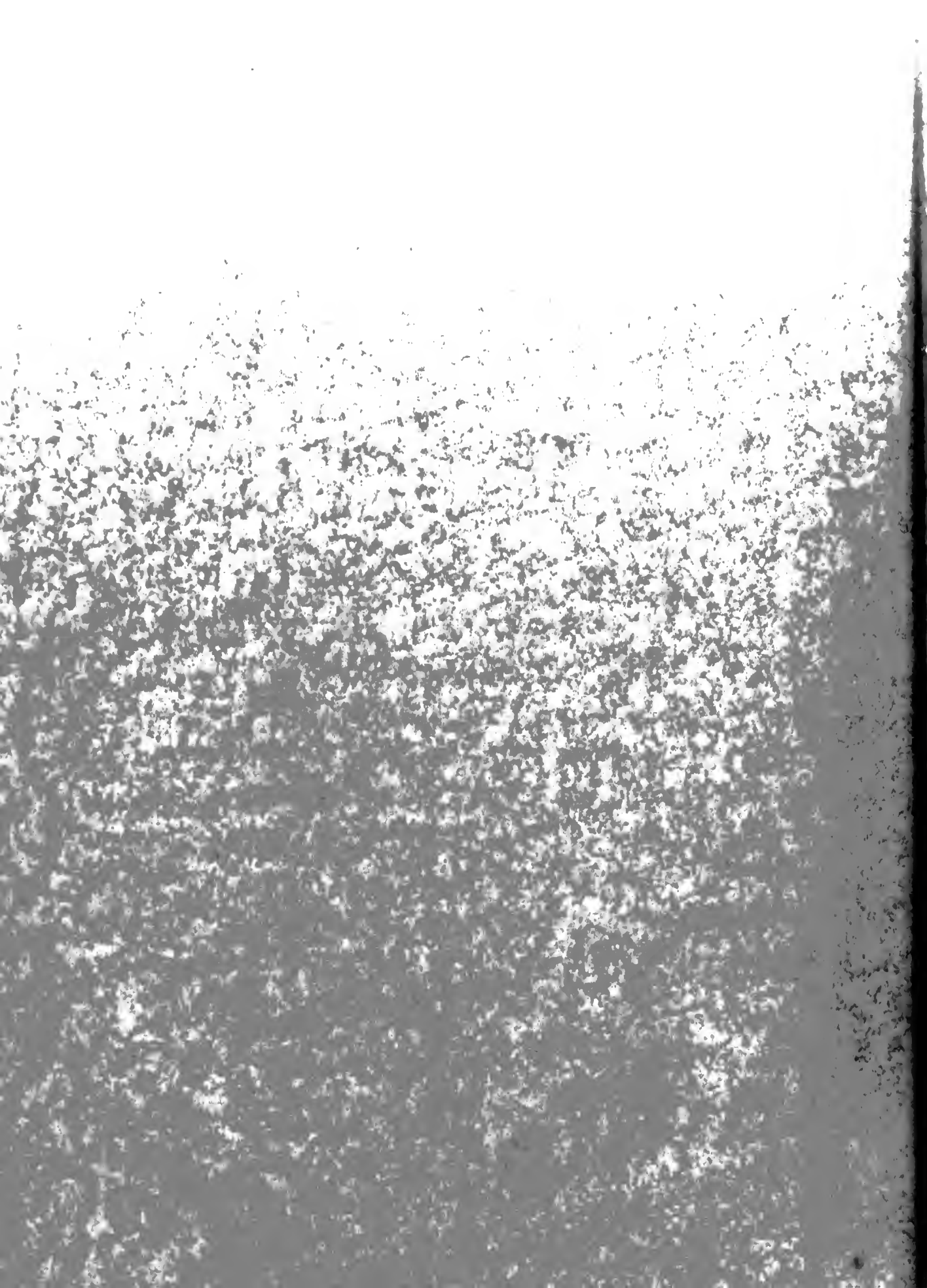

therefore assumed in this section that the angle between ejected neutron and proton from deuterium is constant for coincident protons counted by the proton counter (i.e., for a given proton angle and energy). Thus if a point target were used, the solid angle defined by the proton counter would be reflected in an equal solid angle (at 90° in center of mass coordinates) beam of neutrons arising from the photodisintegration of D. The angular resolution of the experiment would then be simply the angular resolution of the neutron counter. Use of a target of finite dimensions and at an angle to the bremsstrahlung beam results in focusing and defocusing effects that are investigated by numerical methods in this section.

(2) Numerical Analysis

(a) Assumptions on which numerical analysis is based:

1. Angle between neutron and proton ejected is constant over the range of angles included in the proton counter.

2. Bremsstrahlung beam intensity is a Gaussian shape (radial symmetry) clipped by the edge of the collimating system at the $\frac{1}{2}$ maximum value point (this is a very good assumption for the M.I.T. Synchrotron beam). See figure 10a.

3. Finite thickness target can be approximated by a plane target.

4. Loss of neutron counts due to width of counter, figure 10c, can be treated independently from the loss due to height of counter. Figure 10b.

ing and defocusing effects that are investigated by numerical methods in this section.

(2) Numerical Analysis

(a) Assumptions on which numerical analysis is based:

1. Angle between neutron and proton ejected is constant over the range of angles included in the proton counter.

2. Bremsstrahlung beam intensity is a Gaussian shape (radial symmetry) clipped by the edge of the collimating system at the $\frac{1}{2}$ maximum value point (this is a very good assumption for the M.I.T. Synchrotron beam). See figure 10a.

3. Finite thickness target can be approximated by a plane target.

b. Loss of neutron counts due to width of counter, figure 10c, can be treated independently from the loss due to height of counter. Figure 10b.

(b) Method of Analysis

The cross section of the bremsstrahlung beam (2" in diameter at the target) was divided into .2" squares by a grid of perpendicular lines. Each square was assigned a number proportional to the intensity of the bremsstrahlung beam at the center of the square. This number is assumed to be proportional to the number of neutron and proton pairs, $(n+p)_{ij}$, formed in this square. Where i and j refer to its coordinates.

To compute the fraction of the neutrons entering the effective volume of the counter due to dispersion in the vertical direction, lines joining the center of a square and the vertical extremities of the proton counter were extended to intersect a line perpendicular to the neutron counter axis erected at the center of the counter. Consult figure 10 for calculation of a typical square. The ratio of the length of the line segment of the perpendicular to the counter subtended by the vertical height (effective, corrected for side wall losses) of the counter: the length of the segment of this same line that lay between its intersection with the extended lines through the center of the square was determined for each square. This ratio, $(fv)_{ij}$, is assumed to be the fraction of neutrons from the square that arrive in the effective volume of the counter due to divergence (losses) in the vertical direction. Losses due to angular divergence in the horizontal plane due to the finite target were calculated as is shown in the plan view shown in figure 10c. The target length was divided into ten equal segments. The projection of these segments on the plane perpendicular to the beam axis was equal to .2", the size of the grid dividing the

(3) Detector Resolution

The cross section of the streamwise beam (2" in diameter at the target) was divided into .2" squares by a grid of perpendicular lines. Each square was assigned a number proportional to the intensity of the bremsstrahlung beam at the center of the square. This number is assumed to be proportional to the number of neutron and proton pairs, $(n+p)_{ij}$, formed in this square. Where i and j refer to its coordinates.

To compute the fraction of the neutrons entering the effective volume of the counter due to dispersion in the vertical direction, lines joining the center of a square and the vertical extremities of the proton counter were extended to intersect a line perpendicular to the neutron counter axis erected at the center of the counter. Consult figure 10 for calculation of a typical square. The ratio of the length of the line segment of the perpendicular to the counter subtended by the vertical height (effective, corrected for side wall losses) of the counter; the length of the segment of this same line that lay between its intersection with the extended lines through the center of the square was determined for each square. This ratio, $(V)_{ij}$, is assumed to be the fraction of neutrons from the square that arrive in the effective volume of the counter due to divergence (losses) in the vertical direction, losses due to angular divergence in the horizontal plane due to the finite target were calculated as is shown in the plan view shown in figure 10c. The target length was divided into ten equal segments. The projection of these segments on the plane perpendicular to the beam axis was equal to .2", the size of the grid dividing the

Figure 10: Geometric Efficiency factor

Figure 10a shows the assumed intensity of the bremsstrahlung beam as a function of radius. It also shows how the target was divided into squares $(n+p)_{ij}$ by a grid located in a plane perpendicular to the bremsstrahlung beam.

Figure 10b shows the fraction of $(n+p)_{39}$ that enter the effective volume of the counter due to divergence in the vertical direction. This fraction is equal to the ratio of the length of line segments $\frac{\overline{AB}}{\overline{AC}}$.

Figure 10C shows the fraction, $\frac{\overline{RS}}{\overline{RT}}$, of $(n+p)_{39}$ that enter the effective volume of the counter due to divergence in the horizontal direction.

Figure 10 is not to scale and is exaggerated to show clearly what effects are being considered.

clearly what effects are being considered.

Figure 10 is not to scale and is exaggerated to show

the effective volume of the counter due to divergence in the horizontal direction.

Figure 10C shows the fraction, $\frac{\overline{EB}}{\overline{BC}}$, of $(n+p)_{39}$ that enter the vertical direction. This fraction is equal to the ratio of the length of line segments $\frac{\overline{AB}}{\overline{AC}}$.

Figure 10D shows the fraction of $(n+p)_{39}$ that enter the downstream beam.

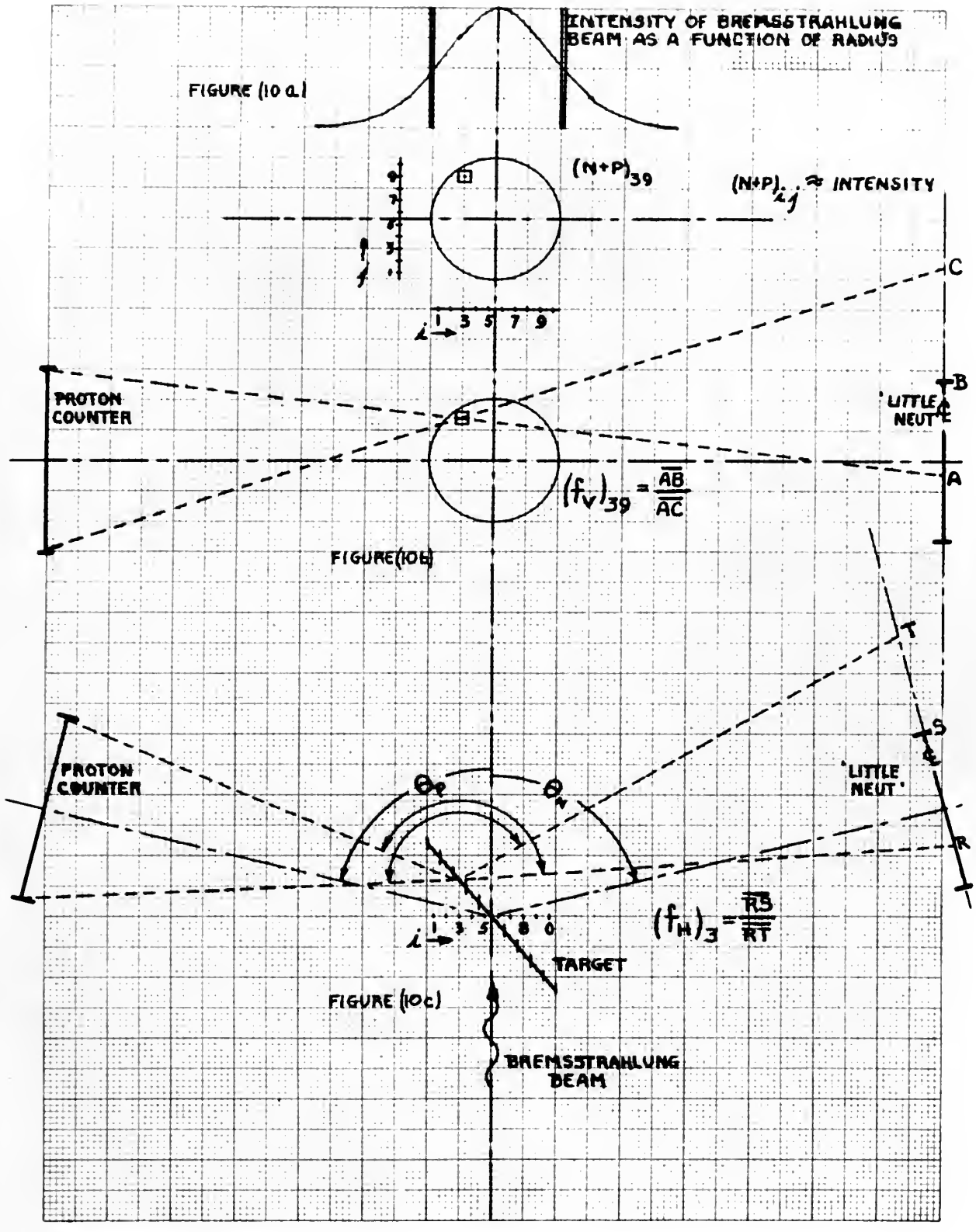
INTENSITY OF BREMSSTRAHLUNG BEAM AS A FUNCTION OF RADIUS
FIGURE (10 a.)
$(N+P)_{39}$
$(N+P)_{ij}$ ≈ INTENSITY
C
B
A
PROTON COUNTER
LITTLE NEUT.
$(f_V)_{39} = \frac{\overline{AB}}{\overline{AC}}$
FIGURE(10b)
T
S
R
PROTON COUNTER
LITTLE NEUT.
θ_P
θ_N
$(f_H)_3 = \frac{\overline{RS}}{\overline{RT}}$
TARGET
FIGURE (10c)
BREMSSTRAHLUNG BEAM

bremsstrahlung beam. A line was drawn from the center of a line segment to one extremity of the proton counter. Another line was drawn at an angle to the first line equal to the angle between the neutron proton pair of the median energy proton accepted. This second line was extended to intersect the perpendicular bisector of the neutron counter as before. A second pair of lines was constructed for the other extremity of the proton counter. As before the ratio of the perpendicular bisector contained in the effective counter: length of the perpendicular bisector between the two lines originating at the proton counter was assumed to be the fraction, $(f_h)_i$ of the neutrons originating in that segment that entered the effective volume of the counter due to divergence in the horizontal plane.

What could be termed a geometrical efficiency factor is then given by the summation $\sum_{ij}(n+p)_{ij}(f_v)_{ij}(f_H)_i$ divided by $\sum_{ij}(n+p)_{ij}$ where the summation is over all the squares.

An analysis with the neutron counter at several angles was carried out for one proton energy and is shown in figure 11.

2. Calculated "Observed" efficiency of "little neut"

a. Efficiency of the counter

The calculation of the efficiency of the small counter is carried out in the same manner as for the FS. The same techniques were employed in computing end effects. Since the physical composition of both liquid scintillators was the same, carbon contribution and cross sections were identical.

b. "Observed" efficiency of "little neut"

The experimental method employed in determining the observed

The experimental method employed in determining the observed

b. "Observed" efficiency of "little rent"

positron and cross sections were identical.

were employed in computing end effects. Since the physical com-

carried out in the same manner as for the ^{32}S. The same techniques

The calculation of the efficiency of the small counter is

a. Efficiency of the counter

2. Calculated "Observed" efficiency of "little rent"

carried out for one proton energy and is shown in figure 11.

An analysis with the neutron counter at several angles was

where the summation is over all the squares.

Given by the summation $\sum_{i=1}^{n} (N+p)_i (f_n)_i^{(N+p)_i}$ divided by $\sum_{i=1}^{n} (N+p)_i$

What could be termed a geometrical efficiency factor is then

of the neutrons originating in that segment that entered the effect-

ive volume of the counter due to divergence in the horizontal plane.

ating at the proton counter was assumed to be the fraction, $(f_n)_i$

length of the perpendicular bisector between the two lines origin-

of the perpendicular bisector contained in the effective counter:

for the other extremity of the proton counter. As before the ratio

neutron counter as before. A second pair of lines was constructed

ond line was extended to intersect the perpendicular bisector of the

neutron proton pair of the median energy proton accepted. This sec-

drawn at an angle to the first line equal to the angle between the

segment to one extremity of the proton counter. Another line was

perpendicular bisector. The line from the center of a line

Figure 11: Angular Resolution of $\frac{n+p}{p}$ events from Deuterium with "Little Henry"

The experimental points were obtained from a D_2O-H_2O subtraction. $E_n = E_p = 129$Mev, $E_{bias} = 10.4$ Mev. The curve is the calculated values of $\frac{n+p}{p}$ for 130 Mev neutrons, $E_{bias} = 10$ Mev.

Fig. No. 7.1 ... $\frac{mp}{p}$ curves from Deuterium with

"Effective Zero"

The experimental points were obtained from a D_2O-H_2O

subtraction. $E_n = S_p = 129Mev$, $E^{Disc}_{n} = 10.4$ Mev.

The curve is the calculated value of $\frac{mp}{p}$ for 130 Mev

neutrons, $E^{Disc}_{n} = 10$ Mev.

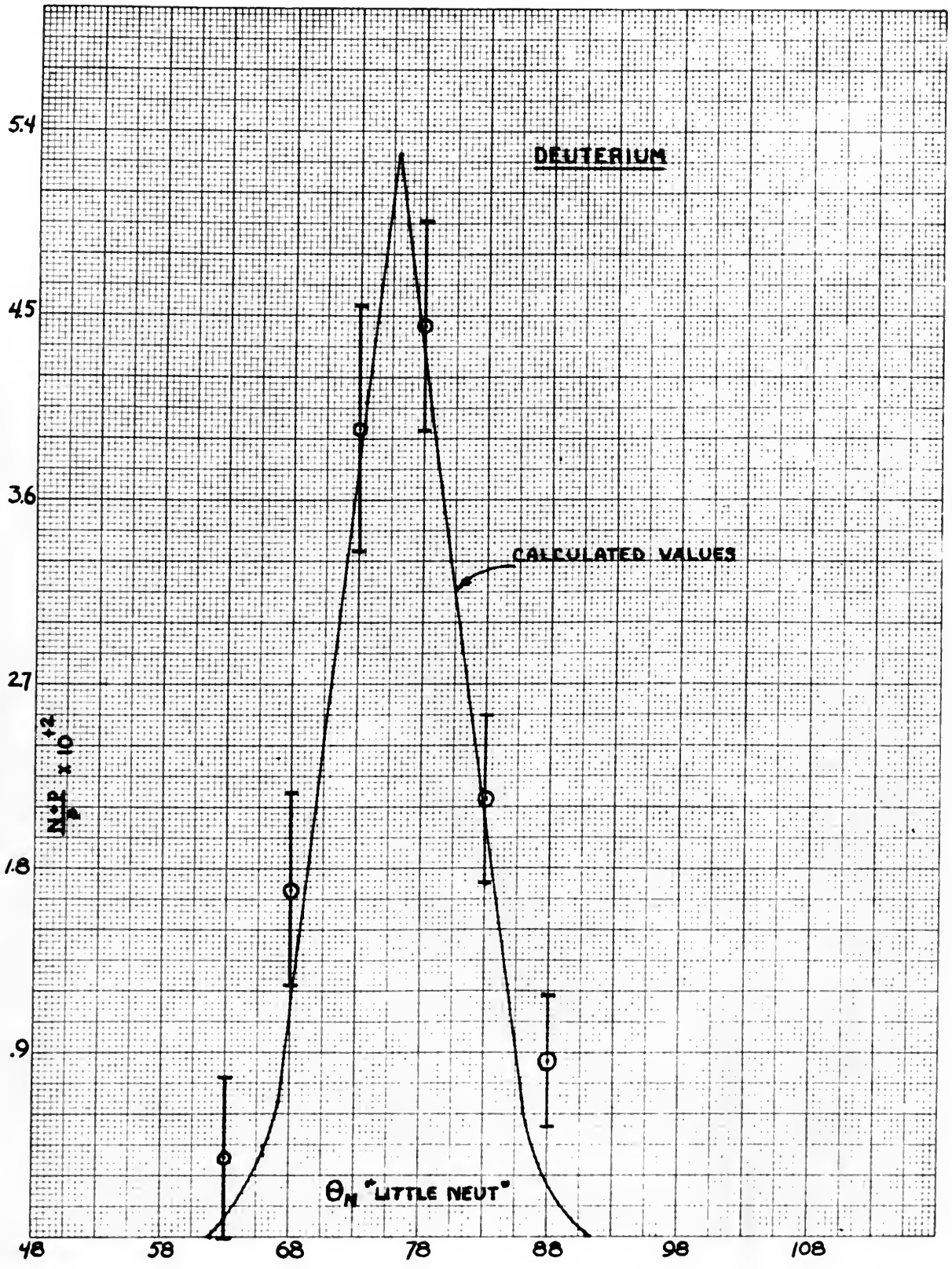
DEUTERIUM
CALCULATED VALUES
θ_N "LITTLE NEUT"
N·P x 10^+2
5.4
4.5
3.6
2.7
1.8
.9
48
58
68
78
88
98
108

Figure 11

efficiency of the counter depended on a D_2O-H_2O subtraction, as is explained in detail in paragraph V,A. This method assumes that the difference between the number of protons (of proper energy) counted from D_2O minus those from H_2O were protons occurring as a result of the photodisintegration of D. In order to compare the calculated "observed" efficiency with that obtained experimentally it is necessary to multiply the neutron counter efficiency obtained above by the fraction of coincident neutrons that enter the effective volume of the counter, paragraph IV, B, 1,b. A further correction is necessary to account for the attenuation of the neutron beam in passing through any shielding material. This is discussed further in the section on experimental results. A plot of calculated "observed" efficiency vs bias for $E_n = 130$ Mev is given in figure 13.

C. Experimental Investigation

The experimental setup for the study of "little neut" is shown in figure 12. As with the FS, the photodisintegration of the deuteron, as obtained from a D_2O-H_2O subtraction, was used as a tool to investigate the characteristics of "little neut". Accidentals were treated in the same manner as they were for the FS. The response of the small counter was determined to be uniform over its entire length by the use of a small Co^{60} source of γ rays. An absolute value for the bias of "little neut" was obtained utilizing the 1.3 Mev γ ray from Co^{60} for a cutoff determination. The bias at the operating point corresponded to a 10.4 Mev electron pulse. The data taken for "little neut" yielded the following information:

efficiency vs bias for $E_n = 1.30$ Mev is given in figure 13.

C. Experimental Investigation

The experimental setup for the study of "little neut" is shown in figure 12. As with the F3, the photodisintegration of the deuteron, as obtained from a D_2O-H_2O subtraction, was used as a tool to investigate the characteristics of "little neut". Accidentals were treated in the same manner as they were for the F3. The response of the small counter was determined to be uniform over its entire length by the use of a small Co^{60} source of γ rays. An absolute value for the bias of "little neut" was obtained utilizing the 1.3 Mev γ ray from Co^{60} for a cutoff determination. The bias at the operating point corresponded to a 10.4 Mev electron pulse. The data taken for "little neut" yielded the following information:

from D_2O minus those from H_2O were protons occurring as a result of the photodisintegration of D. In order to compare the calculated "observed" efficiency with that obtained experimentally it is necessary to multiply the neutron counter efficiency obtained above by the fraction of coincident neutrons that enter the effective volume of the counter, paragraph IV, B, 1,b. A further correction is necessary to account for the attenuation of the neutron beam in passing through any shielding material. This is discussed further in the section on experimental results. A plot of calculated "observed"

difference between the number of protons (of proper energy) counted

explained in detail in paragraph V,A. This method assumes that the efficiency of the counter, governed by a D_2O-H_2O subtraction, is la

Figure 12: Geometry employed in experiments with "Little Neut" Neutron Counter

Figure 12: Geometry employed in experiments with "Little Herb" Neutron Counter

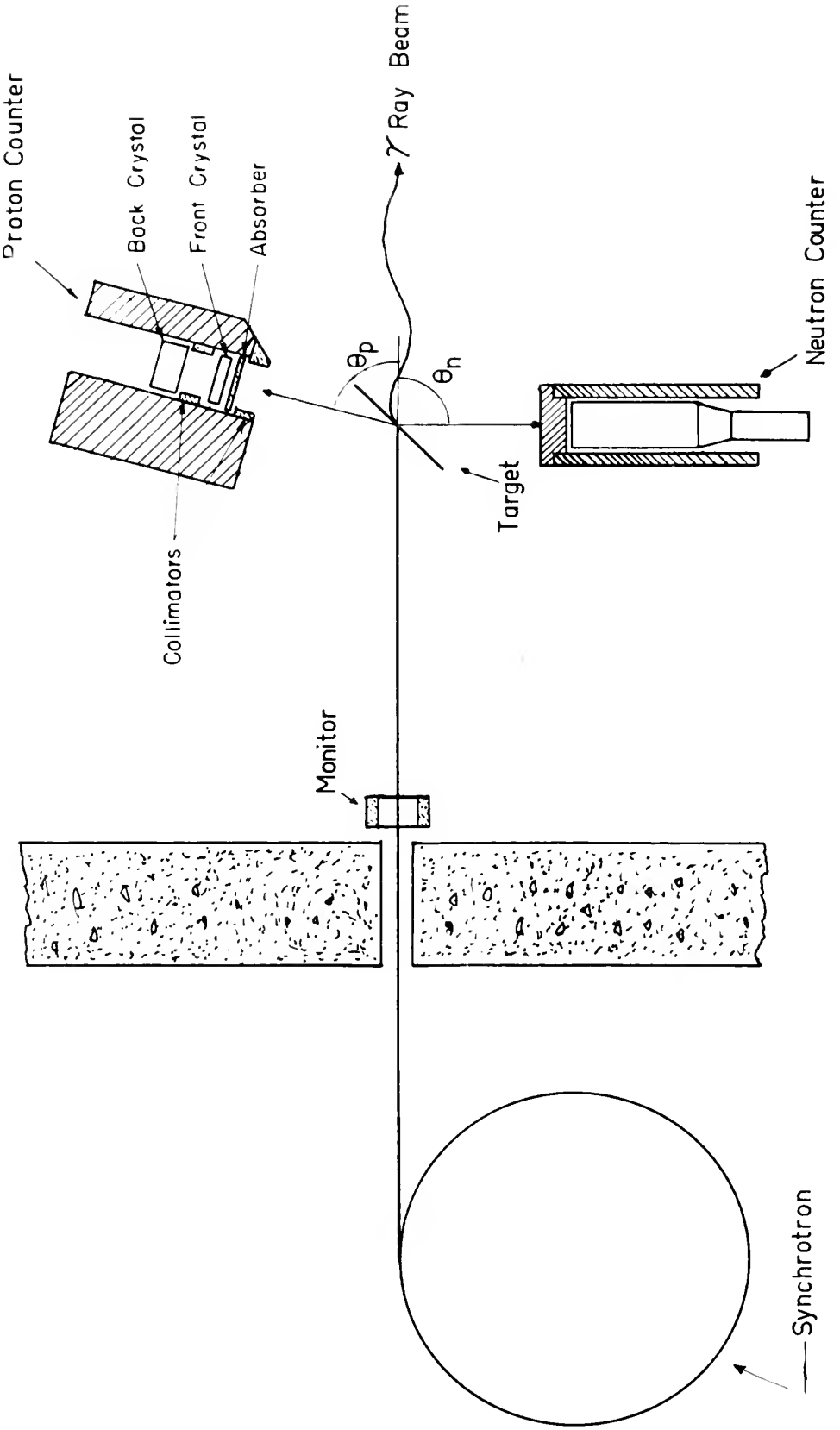
Proton Counter
Back Crystal
Front Crystal
Absorber
γ Ray Beam
Neutron Counter
θp
θn
Target
Collimators
Monitor
Synchrotron

Figure 12

1. Angular Resolution of the Experiment

The angular divergence due to a finite width target was not separated from the undetainty in angle due to the finite size counter. A plot of the angular resolution of the D-photodisintegration experiment is shown in figure 11. The data employed for the experimental points is listed in H. Wilson's thesis.[29] The ratio of n+p events to protons, $\frac{n+p}{p}$, from deuterium is plotted as a function of neutron counter angle. The proton energy was 129 ± 12.5 Mev. The median neutron energy was 129 Mev, median neutron angle 76°, i.e., 90° in the center of mass coordinates.

2. The relative efficiency of "little neut" as a function of bias for E_n = 129 Mev as determined experimentally is shown in figure 13.

D. Discussion of Results

1. Angular Resolution

A calculation of the angular resolution of "little neut" employing the methods described in section IV,B was carried out for the following conditions:

E_γ = 260 Mev	θ_p (avg) = 76°
E_p = 129 ± 12.5 Mev	θ_n (avg) = 76°
E_n = 129 ± 12.5 Mev	$\theta_p^* = \theta_n^*$ = 90° (center of mass coordinates)
(Neutron) E_{bias} = 10 Mev	2" of Pb in front of "little neut"

A calculation of the angular resolution of "little rent" employing the methods described in section IV,B was carried out for the following conditions:

E_γ = 260 Mev	θ_p (ave) = 76°
E_p = 129 ± 12.5 Mev	θ_n (ave) = 76°
E_n = 129 ± 12.5 Mev	$\theta_p = \theta_n = 90°$ (center of mass coordinates)
(Neutron) E_{bias} = 10 Mev	2" of Pb in front of "little rent"

D. Discussion of Results

1. Angular Resolution

2. The relative efficiency of "little rent" as a function of bias for E_n = 129 Mev as determined experimentally is shown in Figure 13.

Figure 13: "Observed" Efficiency of Little Neut vs Bias

The calculated "observed" efficiency of "little neut" as a function of bias for E_n = 130 Mev is given by the curve.

The experimental points are the ratio of n+p coincidence counting rates to proton counting rates, $\frac{n+p}{p}$, from D_2O. These values are normalized to the value of .0529 which was the calculated value for E_{bias} = 10 Mev at the peak of the resolution curve. E_n = 129 Mev.

$E_n = 129$ Mev.

$E_{bias} = 10$ Mev at the peak of the resolution curve.

value of .0529 which was the calculated value for $\frac{n+p}{p}$, from D_2O. These values are normalized to the evidence counting rates to proton counting rates.

The experimental points are the ratio of n+p coin-

the curve.

as a function of bias for $E_n = 129$ Mev is given by

The calculated "observed" efficiency of "little neut"

Figure 13: "Observed" efficiency of little neut vs Bias

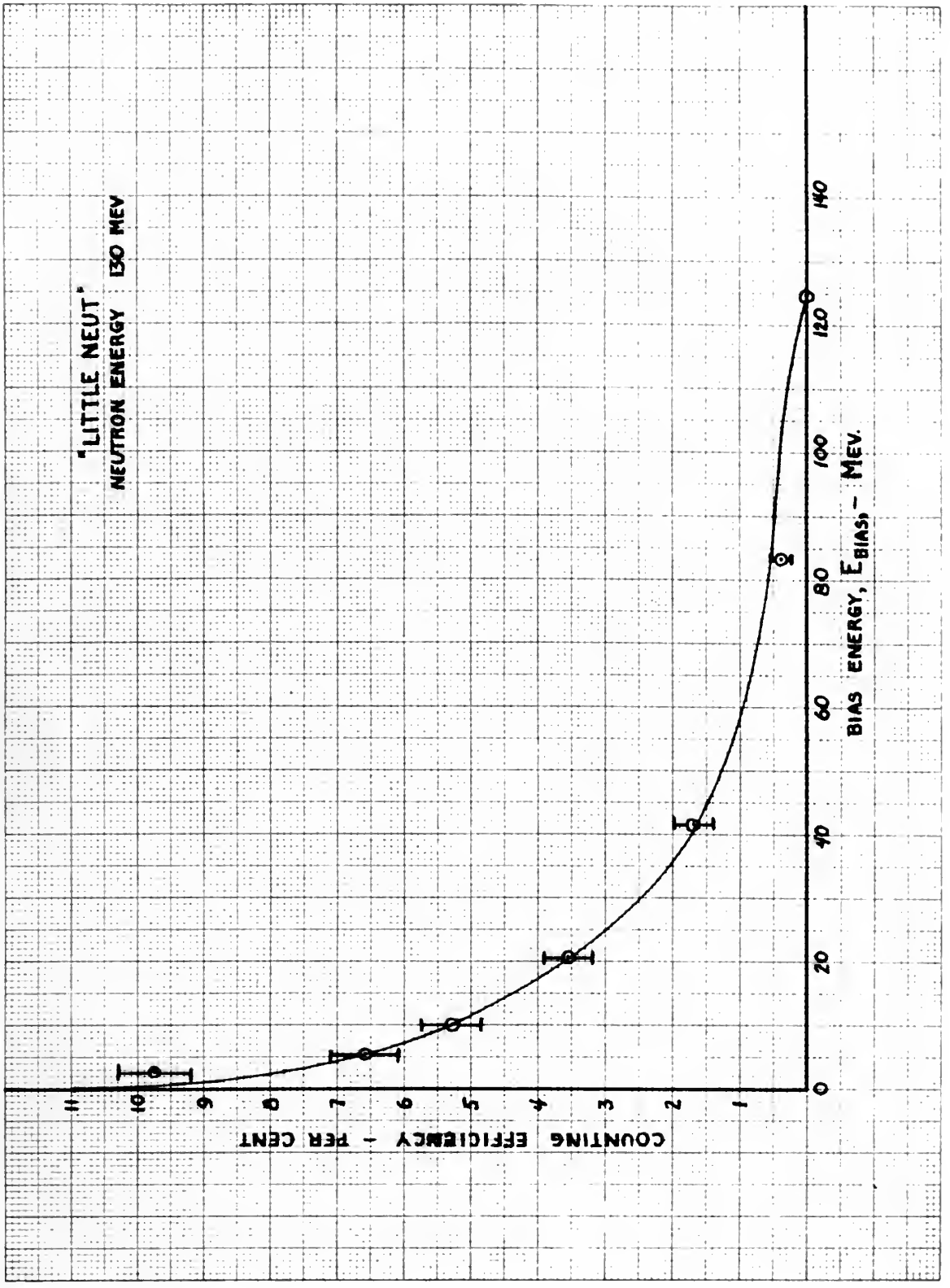
"LITTLE NEUT"
NEUTRON ENERGY 130 MEV
COUNTING EFFICIENCY - PER CENT
BIAS ENERGY, E_{BIAS} - MEV.
0
20
40
60
80
100
120
140
1
2
3
4
5
6
7
8
9
10
11

Figure 13

The curve of figure 11 shows the results of this calculation. The ratio of expected true coincidence counts to proton counts, $\frac{n+p}{p}$, from deuterium is shown as ordinate as a function of the angle, θ_n, between the neutron counter and the bremmstrahlung beam. The curve is normalized to the value obtained in paragraph 2 of this section for the "observed" efficiency at $\theta_n = 76^\circ$. The other calculated points on the curve were obtained by applying the appropriate geometric efficiency (paragraph IV B 1,b) for other values of θ_n as given in the following table:

θ_n	62°	66°	71°	73.5°	76°	78.5°	81°	86°	91°
Geometric Efficiency	.00	.052	.314	.476	.527	.472	.339	.0785	.00

The agreement between the experimental values and the calculated curve, figure 11, is excellent.

Since the neutron counter subtends such a small solid angle, most of the elastic scattering events in the lead will scatter neutrons out of the counter. In the calculations it was assumed that the lead in front of the counter was completely effective in removing neutrons from the beam. Our assumption concerning the lead is not completely valid. Some of the neutrons that are initially headed for the counter and are scattered still enter the effective volume of the counter. Furthermore, since the beam of coincident neutrons from the target is wider than the small counter, some of the neutrons not originally headed for the counter will be scattered into the counter by the 1 1/8" thick lead cylindrical shield surrounding the counter and produce

The curve of Figure II shows the results of this calculation. The ratio of recorded fast coincidence counts to proton counts, $\frac{n_{fc}}{p}$, from deuterium is shown as ordinate as a function of the angle, θ_n, between the neutron counter and the bremsstrahlung beam. The curve is normalized to the value obtained in paragraph 2 of this section for the "observed" efficiency at $\theta_n = 76^\circ$. The other calculated points on the curve were obtained by applying the appropriate geometric efficiency (paragraph IV B 1,b) for other values of θ_n as given in the following table:

θ_n	62°	66°	72°	73.5°	76°	78.5°	81°	86°	91°
Geometric Efficiency	.00	.052	.314	.476	.527	.472	.339	.0785	.00

The agreement between the experimental values and the calculated curve, figure II, is excellent.

Since the neutron counter subtends such a small solid angle, most of the elastic scattering events in the lead will scatter neutrons out of the counter. In the calculations it was assumed that the lead in front of the counter was completely effective in removing neutrons from the beam. Our assumption concerning the lead is not completely valid. Some of the neutrons that are initially headed for the counter and are scattered still enter the effective volume of the counter. Furthermore, since the beam of coincident neutrons from the target is wider than the small counter, some of the neutrons not originally headed for the counter will be scattered into the counter by the 1 1/8" thick lead cylindrical shield surrounding the counter and produce

coincidence counts. To investigate this effect, the increase in $\frac{n+p}{p}$ events from lithium due to an additional 2" of lead surrounding the small counter was measured. Since the angular width of the coincident neutron beam is much wider for lithium than for deuterium, the effect was much larger than for deuterium. The ratio of the solid angles subtended by the lead for (cylindrical shield plus 2" additional): (cylindrical shield) was 5:1. The relative increase in $\frac{n+p}{p}$ events for this condition was 1.4:1. This factor accounts for the experimental values being larger than the calculated values for θ_n near the extremities of the distribution. It also shows that the contribution of neutrons scattered into the counter from the lead shield normally employed was small.

2. Efficiency of "little neut"

The efficiency of both counters depends on a subtraction of counts due to D_2O minus those from H_2O. The n+p coincidences from H_2O must be entirely due to the oxygen. The D_2O and H_2O targets were irradiated for equal flux-times under the same conditions. (The H_2O target was 1.02 times thicker than the D_2O target and in all subtractions the appropriate corrections are made.) The quotient of (number of n+p events from D_2O minus those from corrected H_2O) divided by (the number of protons observed from D_2O minus those from corrected H_2O), i.e., $\frac{\Delta n+p}{\Delta p}$, would give directly an experimental value of the counter efficiency if the neutron counter subtended a sufficient solid angle to include all the neutrons. Since this is not the case for "little neut", an appropriate correction for the loss of neutrons due to the geometry employed must be made in order to compare predicted

to the geometry employed must be made in order to compare predicted counter efficiency if the neutron counter subtended a sufficient solid angle to include all the neutrons. Since this is not the case for "little rest", an appropriate correction for the loss of neutrons due

$$\frac{\Delta n+p}{\Delta p}$$

, i.e., would give directly an experimental value of the (number of n+p events from D_2O minus those from corrected H_2O) divided by (the number of protons observed from D_2O minus those from corrected H_2O). The quotient of subtractions the appropriate corrections are made.) The quotient of were irradiated for equal flux-times under the same conditions. (The H_2O target was 1.02 times thicker than the D_2O target and in all H_2O must be entirely due to the oxygen. The D_2O and H_2O targets counts due to D_2O minus those from H_2O. The n+p coincidences from

2. Efficiency of "little rest"

The efficiency of both counters depends on a subtraction of normally employed was small.

bution of neutrons scattered into the counter from the lead shield the extremities of the distribution. It also shows that the experimental values being larger than the calculated values for θ' near for this condition was 1.1:1. This factor accounts for the (cylindrical shield) was 5:1. The relative increase in $\frac{n+p}{p}$ events subtended by the lead for (cylindrical shield plus 2" additional) was much larger than for deuterium. The ratio of the solid angles neutron beam is much wider for lithium than for deuterium, the effect all counts were measured. Since the angular width of the coincident

value of $\frac{n+p}{p}$ [illegible] experimentally. The geometric correction is considered in the section concerning angular resolution of "little neut".

For convenience we will refer to the ratio of n+p events to p events from deuterium as the "observed" efficiency. The efficiency of the proton counter is ~100%. The calculated "observed" efficiency is a function of three factors: (1) counter efficiency, (2) geometric efficiency factor, (3) attenuation of neutron beam due to shielding.

For the conditions given in the preceding paragraph the calculated numerical values obtained for the "observed" efficiency at the maximum value were:

0.183 (calculated counter efficiency)	x	0.527 (geometric efficiency)	x	0.548 (attenuation factor)	=	0.0529 ("observed" efficiency)

The agreement between the calculated values and experimental absolute values, which is shown in figure 11, is good. Figure 11 is actually a plot of "observed" efficiency vs neutron counter angle.

A comparison of calculated and experimental "observed" efficiencies of "little neut" vs neutron bias for a neutron energy of 130 Mev is shown in figure 13. The experimental points are the ratio of the counting rate of n+p coincidences to the counting rate of proton events, $\frac{n+p}{p}$, from B_2O. The experimental values are normalized to the calculated value of "observed" efficiency obtained for a bias of 10 Mev.

[illegible] of "little rest".

For convenience we will refer to the ratio of n+p events to p events from neutrons as the "observed" efficiency. The efficiency of the proton counter is ~1.00. The calculated "observed" efficiency is a function of three factors: (1) counter efficiency, (2) geometric efficiency factor, (3) attenuation of neutron beam due to shielding.

For the condition given in the preceding paragraph the calculated numerical values obtained for the "observed" efficiency at the maximum value were:

(calculated counter efficiency)	x	(geometric efficiency)	x	(attenuation factor)	=	("observed" efficiency)
0.183	x	0.577	x	0.248	=	0.0529

The agreement between the calculated values and experimental absolute values, which is shown in figure 11, is good. Figure 11 is actually a plot of "observed" efficiency vs neutron counter angle.

A comparison of calculated and experimental "observed" efficiencies of "little rest" vs neutron bias for a neutron energy of 1.30 Mev is shown in figure 13. The experimental points are the ratio of the counting rate of n+p coincidences to the counting rate of proton events, $\frac{n+p}{p}$, from Fig 6. The experimental values are normalized to the calculated value of "observed" efficiency obtained for a bias of 10 Mev.

V. CONCLUSION

A. Efficiency

The efficiency is obtained from experimental data by taking the ratio of n+p coincidence counts to (single) proton counts from deuterium. The denominator of this ratio is a small difference between two large numbers (protons_{D_2O} — protons_{H_2O}). This is an unhappy situation in that it yields a final experimental result with a large statistical uncertainty. In view of the consistency of the calculated efficiencies compared to those obtained experimentally, it is felt that the calculated values are probably as reliable as the experimental values. The reliability of the calculated values is of course dependent on the accuracy with which the neutron cross sections employed in the calculations are known.

The experimental determination of efficiencies should be repeated with the liquid deuterium target when it becomes available to remove the ambiguity associated with the subtraction method. If this were done the experimental results could be made more reliable than the calculations.

B. Angular Resolution

The data on the angular resolution is good. The agreement between the calculated values and experimental points in the case of "little neut" supports our confidence in the reliability of angular distributions obtained with the use of "little neut". Careful curve shapes of differential cross section can be obtained with "little neut" and are given in references 5 and 29 for several different target nuclei.

A. Efficiency

The efficiency is obtained from experimental data by taking the ratio of ntp coincidence counts to (single) proton counts from deuterium. The denominator of this ratio is a small difference between two large numbers (protons$_{D_2O}$ -- protons$_{H_2O}$). This is an unhappy situation in that it yields a final experimental result with a large statistical uncertainty. In view of the consistency of the calculated efficiencies compared to those obtained experimentally, it is felt that the calculated values are probably as reliable as the experimental values. The reliability of the calculated values is of course dependent on the accuracy with which the neutron cross sections employed in the calculations are known.

The experimental determination of efficiencies should be repeated with the liquid deuterium target when it becomes available to remove the ambiguity associated with the subtraction method. If this were done the experimental results could be made more reliable than the calculations.

B. Angular Resolution

The data on the angular resolution is good. The agreement between the calculated values and experimental points in the case of "little meut" supports our confidence in the reliability of angular distributions obtained with the use of "little meut". Characteristic curve shapes of differential cross section can be obtained with "little meut" and are given in references 5 and 29 for several different target nuclei.

C. [illegible]

In order to compare the data obtained in different experiments or by different detectors one needs to know the absolute values of the efficiencies of the detectors employed. From the analysis of the angular focusing and defocusing of targets performed in this thesis one can obtain experimentally the efficiency of the detectors from the data on the photodisintegration of the deuteron.

One has much more confidence in the experimentally obtained values of the efficiency if one can estimate the efficiency from a knowledge of the fundamental nuclear reactions involved. It is therefore very satisfying to find that there is agreement in the values of the efficiencies obtained experimentally and the values calculated. The excellence of the agreement for the small counter (shown in figure 11) to some extent must be fortuitous.

D. Summary

This thesis has attempted to clarify the factors involved in measuring or calculating the efficiency of high energy neutron detectors. The more important of these factors and their interplay on one another are listed:

1. Target size and settings can cause focusing and defocusing effects in coincidence measurements.

2. The lead shielding in front of a small counter attenuates the neutron beam but may not do so on a large counter depending on the bias employed. The lead shielding on the side of a counter is not too important if it is kept thin, its main effect is that it adds

In order to compare the data obtained in different experiments by different detectors one needs to know the absolute values of the efficiencies of the detectors employed. From the analysis of the angular focusing and defocusing of targets performed in this thesis one can obtain experimentally the efficiency of the detectors from the data on the photodisintegration of the deuteron.

One has much more confidence in the experimentally obtained values of the efficiency if one can estimate the efficiency from a knowledge of the fundamental nuclear reactions involved. It is therefore very satisfying to find that there is agreement in the values of the efficiencies obtained experimentally and the values calculated. The excellence of the agreement for the small counter (shown in figure 11) to some extent must be fortuitous.

D. Summary

This thesis has attempted to clarify the factors involved in measuring or calculating the efficiency of high energy neutron detectors. The more important of these factors and their interplay on one another are listed:

1. Target size and settings can cause focusing and defocusing effects in coincidence measurements.

2. The lead shielding in front of a small counter attenuates the neutron beam but may not do so on a large counter depending on the bias employed. The lead shielding on the side of a counter is not too important if it is kept thin, its main effect is that it adds

a small bail on the angular resolution of the detector.

3. The star and spallation fragments from carbon in the scintillating liquids contribute an increasingly larger fraction of the events observed as one lowers the bias of the detector.

4. The efficiency as a function of the discriminator bias depends upon the size of the neutron counter. In a small counter the efficiency is much more readily predictable as a function of bias. The simple dependence expected from isotropic proton recoils does not hold at these high energies because of factors 2 and 3 discussed above.

5. The efficiency as a function of the energy of the neutrons has not been satisfactorily predicted. More information is needed concerning variation of the number of star and spallation fragments as a function of neutron energy. Additional information is also needed on the various differential cross-sections of neutrons on lead.

In future experiments on detectors, the efficiency should not be determined by a subtraction method.

a small part of the angular resolution of the detector.

3. The star and scattering fragments from carbon in the scintillating liquids contribute an increasingly larger fraction of the events observed as one lowers the bias of the detector.

4. The efficiency as a function of the discriminator bias depends upon the size of the neutron counter. In a small counter the efficiency is much more readily predictable as a function of bias. The simple dependence expected from isotropic proton recoils does not hold at these high energies because of factors 2 and 3 discussed above.

5. The efficiency as a function of the energy of the neutrons has not been satisfactorily predicted. More information is needed concerning variation of the number of star and spallation fragments as a function of neutron energy. Additional information is also needed on the various differential cross-sections of neutrons on lead.

In future experiments on detectors, the efficiency should not be determined by a subtraction method.

REFERENCES

1. B. T. Feld, V. D. Godbole, A. Odian, P. Scherb, P. C. Stein, and A. Wattenberg: Phys. Rev. 94,1000 (1954) This paper gives references to similar work at other laboratories.

2. H. Meyers, A. Odian, P. C. Stein, and A. Wattenberg: Phys. Rev. 95, 57 (1954)

3. N. C. Barton and J. H. Smith: Phys. Rev. 95, 573 (1954)

4. J. S. Levinger: Phys. Rev. 84, 43 (1951)

5. A. Odian: M.I.T. Doctoral Thesis, June 1955, to be published

6. J. DeJuren and B. J. Moyer: Phys. Rev. 81, 919 (1951)

7. Taylor and Wood: Phil Mag. 44, 95 (1953)

8. L. E. Beghian and H. Halben: Proc. Phys. Soc. (London) 62A,395 (1949)

9. C. R. Sun and J. Reginald Richardson: Rev. Sci. Inst. 25, 691 (1954)

10. M. A. Van Dilla: Phys. Rev. 85, 705 (1952)

11. J. R. Holt and A. E. Sutherland: Rev. Sci. Inst. 25,298 (1954)

12. F. J. Hughes and C. Eggler: Phys. Rev. 72, 902 (1947)

13. G. R. Keepin,jr. and J. H. Roberts: Phys. Rev. 76, 154 (1949) Rev. Sci. Inst. 21, 163 (1950)

14. J. DeSuren and N. Knable: Phys. Rev. 77, 606 (1950)

15. C. Wiegand: Rev. Sci. Inst. 19, 790 (1948)

16. H. Kallman and M. Furst: Phys. Rev. 79, 857 (1950); Phys. Rev. 81, 853 (1951); Nucleonics March, 1951 p.32

17. R. K. Swank and W. L. Buck: Rev. Sci. Inst. 26, 15 (1955)

18. J. B. Birks: Phys. Rev. 84, 364 (1951); Phys, Rev. 86, 569 (1952)

19. C. J. Taylor, W. K. Jenkschke, M. E. Remley, R. S. Eby, and P. G. Kruger: Phys. Rev. 84, 1034 (1951)

20. D. A. Kellogg: Phys. Rev. 90, 224 (1953); UCRL 1899

21. J. Hadley and H. York: Phys. Rev. 80, 345 (1950)

BIBLIOGRAPHY

1. D. A. Vela, ... Gaskell, W. Watson, W. Bowers, T. C. Stelle, and ... Rattenberg: Rhys. Rev. 91, 1000 (1953). This paper gives references to similar work at other laboratories.

2. E. Fayard, A. Gozlan, A. C. Stein, and A. Rattenberg: Phys. Rev. 95, 57 (1953).

3. M. C. Barton and C. H. Smith: Phys. Rev. 95, 573 (1953).

4. J. S. Levinger: Phys. Rev. 81, 43 (1951).

5. A. Gozlan: M.I.T. Doctoral Thesis, June 1955, to be published

6. J. Delaren and B. J. Moyer: Phys. Rev. 81, 919 (1951)

7. Taylor and Wood: Phil Mag. 44, 95 (1953)

8. L. E. Beghian and E. Melben: Proc. Phys. Soc. (London) 62A,395 (1949)

9. C. R. Sun and J. Reginald Richardson: Rev. Sci. Inst. 25, 691 (1954)

10. M. A. Van Dilla: Phys. Rev. 85, 705 (1952)

11. J. R. Holt and A. J. Sutherland: Rev. Sci. Inst. 25,298 (1954)

12. F. J. Hughes and C. Leffler: Phys. Rev. 72, 902 (1947)

13. G. R. Keepin,Jr. and J. R. Roberts: Phys. Rev. 76, 1514 (1949) Rev. Sci. Inst. 21, 163 (1950)

14. J. Delaren and E. Knable: Phys. Rev. 77, 606 (1950)

15. C. Wiegand: Rev. Sci. Inst. 19, 790 (1948)

16. E. Hallman and M. Furst: Phys. Rev. 79, 857 (1950); Phys. Rev. 81, 853 (1951); Nucleonics March, 1951 p.32

17. E. E. Swank and W. L. Buck: Rev. Sci. Inst. 26, 15 (1955)

18. J. B. Birks: Phys. Rev. 81, 1014 (1951); Phys. Rev. 86, 569 (1952)

19. C. J. Taylor, J. K. Jenkenshire, R. J. Manley, E. B. Eby, and P. C. Kruger: Phys. Rev. 81, 1034 (1951)

20. D. A. Kellogg: Phys. Rev. 90, 224 (1953); UCRL 1899

21. J. Medley and H. York: Phys. Rev. 80, 315 (1950)

22. E. Kelly, C. Leith, E. Segre, and C. Wiegand: Phys. Rev. 79, 96 (1950)

23. H. Kahn: Nucleonics, May, 1950 p.27; June 1950, p.60

24. Nat'l Bureau of Standards Publication NBS-12

25. J. W. Draper: Rev. Sci. Inst. 25, 558 (1954)

26. A. Wattenberg: Ann. Rev. of Nuc. Sci. 3, 119 (1953)

27. M. R. Cleland: Nat'l Bureau of Standards Report 2036, (NBS Project 3300-30-7507) (1952)

28. F. Reines, C. L. Cowan,jr., F. B. Harrison, and D. J. Carter: Rev. Sci. Inst. 25, 1061 (1954)

29. M. Rich and R. Madey: UCRL 2301 (1954)

30. H. Wilson: M.I.T. Masters Thesis June,1955

31. A. Wattenberg: Appended to Reference 30, to be published

[illegible]. [illegible], [illegible]. Geophysics 15, 75, 96 (1950)

[illegible]. [illegible] Electronics, New. 195 pp.17 June 1950, p.60

[illegible] Nat'l Bureau of Standards Circular 590-12

1. ... Proper: Rev. Sci. Instr. 25, 558 (1954)

A. Wattenberg: Ann. Rev. of Nuc. Sci. 3, 119 (1953)

M. R. Cleland: Nat'l Bureau of Standards Report 2036, (NBS Project 3300-30-7507) (1951)

T. Baines, C. L. Cowan, Jr., E. B. Harrison, and D. A. Carter: Rev. Sci. Inst. 25, 1001 (1954)

H. Hlob and R. Maley: UCRL 2301 (1954)

N. Wilson: M.I.T. Masters Thesis June, 1955

A. Wattenberg: Appended to References 30, to be published

28912

C474 Thesis

Christie
A Study of high energy
neutron detectors.